Zonal circulation across 52°W in the North Atlantic

Melinda M. Hall, Terrence M. Joyce, and Robert S. Pickart
Physical Oceanography Department, Woods Hole Oceanographic Institution, Woods Hole, Massachusetts, USA

William M. Smethie Jr.
Lamont-Doherty Earth Observatory, Columbia University, Palisades, New York, USA

Daniel J. Torres
Physical Oceanography Department, Woods Hole Oceanographic Institution, Woods Hole, Massachusetts, USA

Received 21 August 2003; revised 3 June 2004; accepted 19 July 2004; published 18 November 2004.

[1] In July–August 1997, a hydrographic/Acoustic Doppler Current Profiler (ADCP)/tracer section was occupied along 52°W in the North Atlantic as part of the World Ocean Circulation Experiment Hydrographic Program. Underway and lowered ADCP (LADCP) data have been used to reference geostrophic velocities calculated from the hydrographic data; additional (small) velocity adjustments provided by an inverse model, constraining mass and silicate transports in 17 neutral density layers, yield the absolute zonal velocity field for 52°W. We find a vigorous circulation throughout the entire section, with an unusually strong Gulf Stream (169 Sv) and southern Deep Western Boundary Current (DWBC; 64 Sv) at the time of the cruise. At the northern boundary, on the west side of the Grand Banks of Newfoundland, we find the westward flowing Labrador Current (8.6 Sv), whose continuity from the Labrador Sea, east of our section, has been disputed. Directly to the south we identify the slopewater current (12.5 Sv eastward) and northern DWBC (12.5 Sv westward). Strong departures from strictly zonal flow in the interior, which are found in the LADCP data, make it difficult to diagnose the circulation there. Isolated deep property extrema in the southern portion, associated with alternating bands of eastward and westward flow, are consistent with the idea that the rough topography of the Mid-Atlantic Ridge, directly east of our section, causes enhanced mixing of Antarctic Bottom Water properties into overlying waters with distinctly different properties. We calculate heat and freshwater fluxes crossing 52°W that exceed estimates based on air-sea exchanges by a factor of 1.7. *INDEX TERMS:* 4532 Oceanography: Physical: General circulation; 4536 Oceanography: Physical: Hydrography; 4576 Oceanography: Physical: Western boundary currents; *KEYWORDS:* North Atlantic Circulation, Gulf Stream, Deep Western Boundary Current

Citation: Hall, M. M., T. M. Joyce, R. S. Pickart, W. M. Smethie Jr., and D. J. Torres (2004), Zonal circulation across 52°W in the North Atlantic, *J. Geophys. Res.*, *109*, C11008, doi:10.1029/2003JC002103.

1. Introduction

[2] In summer of 1997, two meridional hydrographic sections were occupied in the North Atlantic, as part of the World Ocean Circulation Experiment (WOCE) Hydrographic Program's (WHP) survey of the world ocean. The main objectives of this work were to obtain a quantitative description of the North Atlantic circulation and water mass distribution in the mid-1990s; to compare this state to similar basin-wide descriptions from two previous eras, the IGY period (late 1950s to early 1960s) and the early 1980s; and to characterize these snapshots in terms of climate variability. Because the expected magnitude of variations in surface heating is expected to be small compared to present uncertainties in those measurements, the best present indicator of climate change is in directly observed variations of heat/salt/tracer inventories of the ocean basin [see, e.g., *Joyce and Robbins*, 1996]. The two meridional lines that were occupied are crucial in diagnosing such changes for two reasons: first, they span the entire subtropical gyre, providing WOCE era measurements of the meridional structure of the major zonal flows (e.g., the Gulf Stream), as well as tracers that have been injected into recirculation gyres; and second, together they provide four individual crossings of the western boundary currents, which are key to the propagation and feedback of climate signals. *Joyce et al.* [2001] have reported on the 66°W line, and *Joyce et al.* [1999] examined decadal changes in the hydrographic structure of both lines, using the IGY sections from the 1950s and sections from the 1980s for comparison.

[3] The R/V *Knorr* departed Halifax, Nova Scotia, on 17 July, steamed eastward to the Grand Banks southeast of

0148-0227/04/2003JC002103$09.00

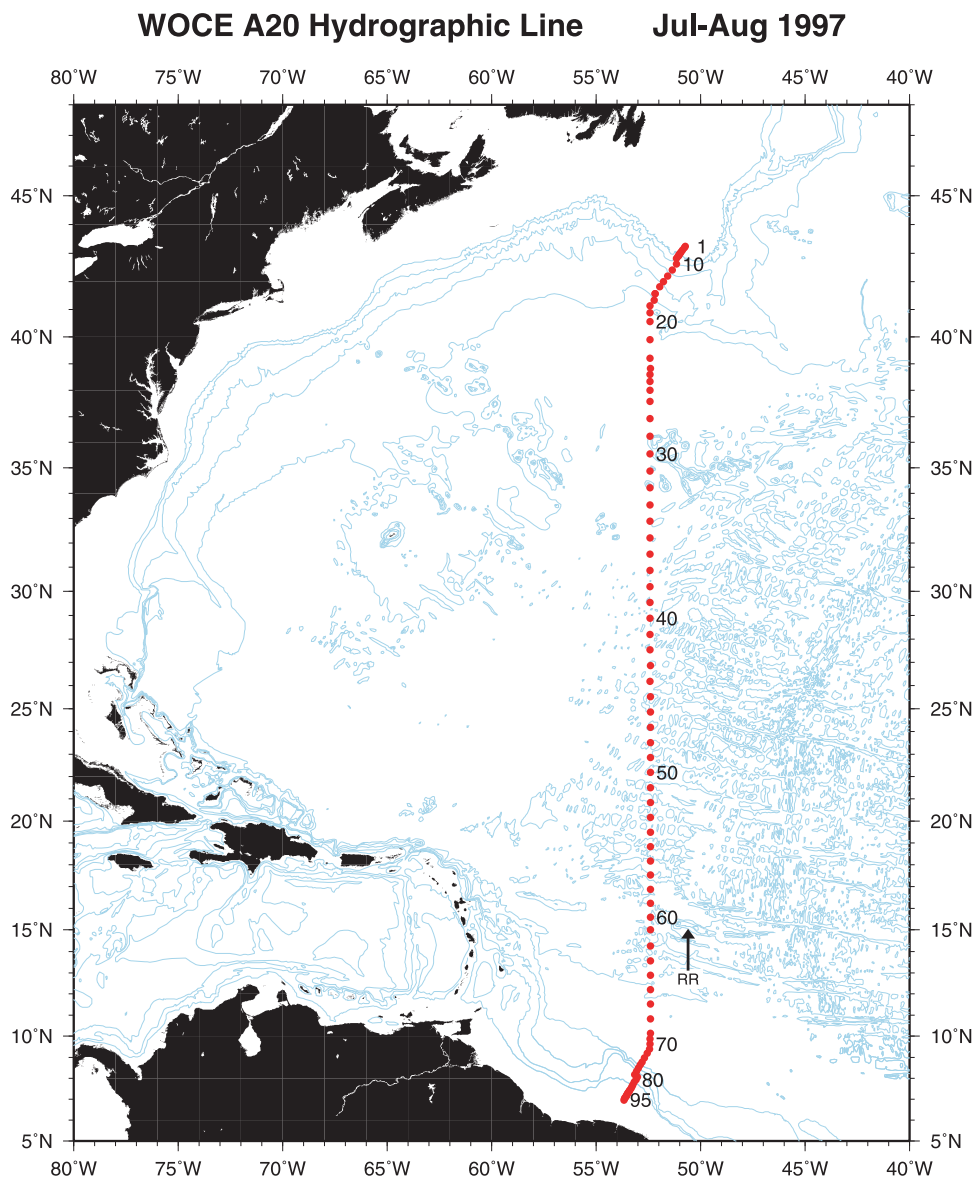

Figure 1. Cruise track for WOCE section A20, superposed on topography: topographic contours are every 1000 m. Red dots are station positions, with some stations numbers indicated. "RR" indicates the location of Researcher Ridge (shallower than 3000 m).

Newfoundland, then headed south along 52°20′W (see Figure 1), finishing the hydrographic work off the coast of Suriname. Following a port stop in Trinidad, the ship then worked northward nominally along 66°W back to the continental shelf south of Cape Cod, Massachusetts. All data were collected to WOCE standards [*Joyce*, 1994]; details of calibrations and nutrient analyses may be found online at http://whpo.ucsd.edu. Lowered and underway acoustic Doppler current profiler (ADCP) data were also collected during both cruises, though some difficulties were encountered with the lowered ADCP on the 52°W leg, as discussed below.

[4] In this paper we first present the hydrographic and LADCP data collected on the 52°W cruise (section 2), as well as chlorofluorocarbons (CFCs). We then use the hydrographic data in conjunction with both the lowered and shipboard ADCP data (LADCP and SADCP, respectively) to describe the zonal circulation across the 52°W meridian. The development of this paper roughly follows that laid out in the work of *Joyce et al.* [2001] for ease of intercomparison between the 52°W and 66°W sections. In section 3 the underway and lowered ADCP data are described, including the aforementioned difficulties with the latter. This section also compares the LADCP, SADCP and geostrophic velocity shears, and discusses the choice of reference level velocity for the latter, based on these comparisons. In section 4, following *Joyce et al.* [2001], we use an inverse model to determine an absolute velocity field along the section. The starting point for the inverse is the velocity field determined in section 3; conservation constraints on mass and silicate fluxes are then imposed, requiring a barotropic velocity adjustment for each station pair, which is determined by the inverse. This circulation is discussed in terms of the meridional mass transport stream

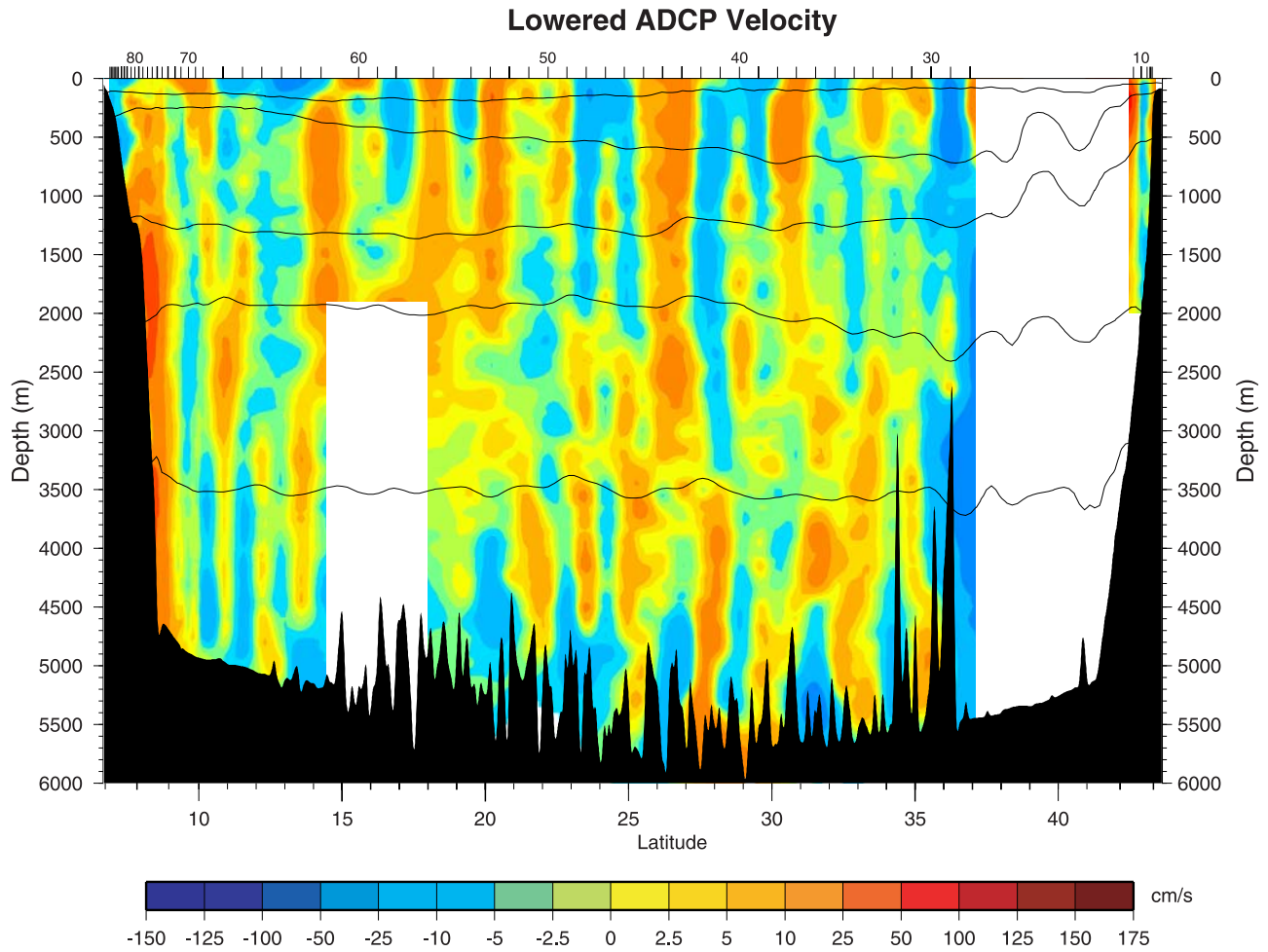

Figure 2. LADCP velocities perpendicular to A20 track line; positive velocities have eastward component. Blank areas are those where no LADCP data are available.

functions for 6 different density layers in Section 5, and the associated heat and freshwater fluxes are discussed in Section 6.

2. Data Description

[5] We began our section near the 80 m isobath at 43°14.8′N, 50°37.01′W (Figure 1). No bottle data were collected for the first five stations, which all lay in less than 200 m of water. The line followed a dogleg southwest across the northern boundary current system and a warm core Gulf Stream ring, then headed due south along 52°20′W at station 19 (43°52.6′N). This continued until we neared the continental rise at the southern end (station 72, 9°11.8′N), where another gentle dogleg to the southwest was followed until we reached the 75 m isobath at 6°58.1′N. Figure 1 shows the station positions superimposed on the topography: stations were more closely spaced over steep topography (i.e., near the boundaries) and across the Gulf Stream. In the interior portions, spacing was 75 km (40 min of latitude). In all, 95 conductivity-temperature-depth (CTD) stations were occupied, and bottle data were collected for stations 6 through 95, using a 36-position rosette mounted with 10-L bottles, though problems partway through the cruise reduced our vertical sampling density to 33 bottles. In addition, a lowered ADCP (LADCP) package mounted on the CTD frame collected data for most stations, with exceptions as noted in section 3. There are only 94 distinct stations: station 16 was essentially a repeat of station 15, required because on station 15 only bottles below 3000 db tripped.

[6] Figure 2 shows the component of LADCP velocity perpendicular to the cruise track. Figures 3a–3h display vertical sections of potential temperature (ϑ), salinity, neutral density (γ), dissolved oxygen, nitrate, phosphate, silicate, and CFC-11. The temperature and density sections (Figures 3a and 3c) do not contain the rich structure visible in other property variables, but they do reveal the most prominent dynamical features along the section. The deep western boundary current (DWBC) is visible at the northern end of the section in the rise of deep isopycnals and isotherms ($\vartheta \sim 1.9°–4.0°$C) toward the boundary, as well as elevated levels of dissolved oxygen and CFC-11 (Figures 3d and 3h). North of station 11, the cold, relatively fresh water above 300 m is in the westward extension of the equatorward flowing Labrador Current. The warmer, more saline waters immediately offshore of this comprise the eastward flowing slopewater current: this is a minor bifurcation of the Gulf Stream that branches off near 60°W [*Csanady and Hamilton*, 1988; *Pickart et al.*, 1999]. In

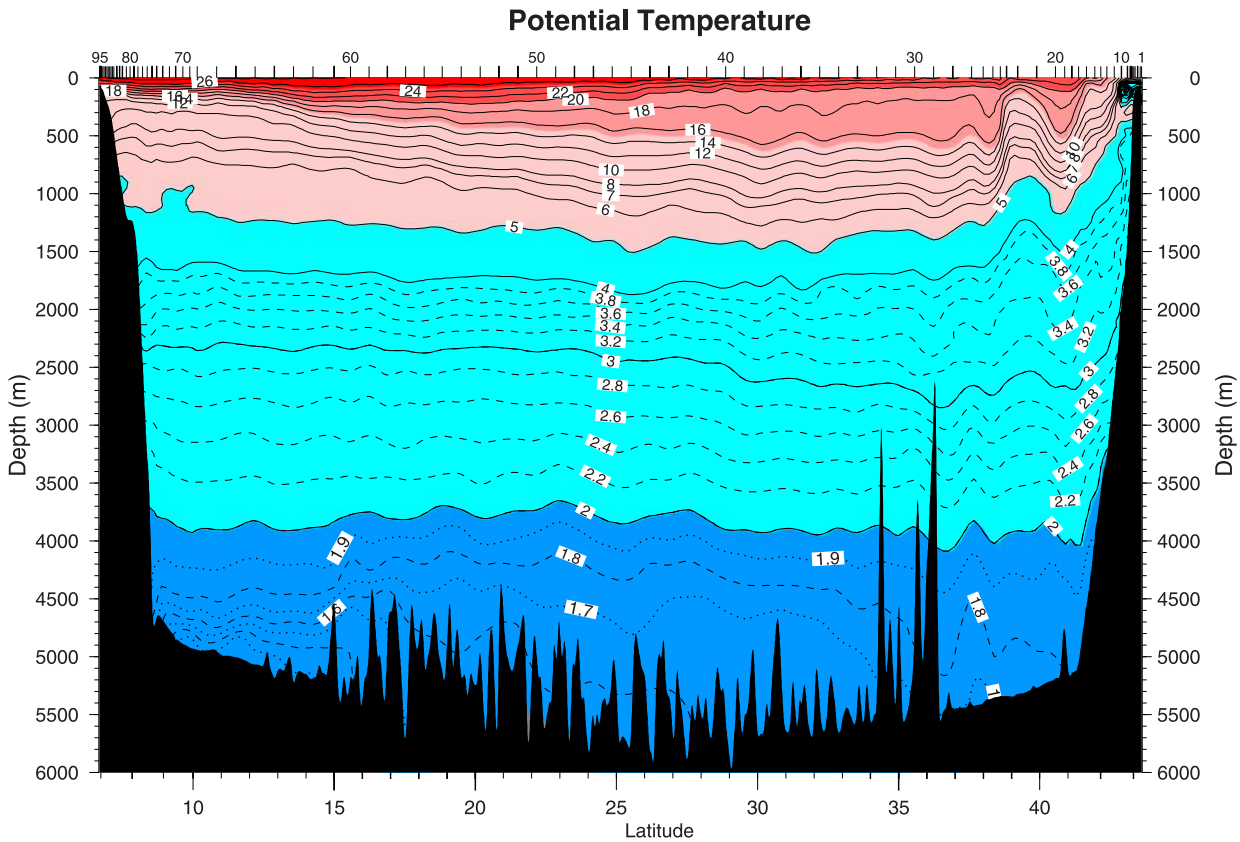

Figure 3a. Potential temperature (°C).

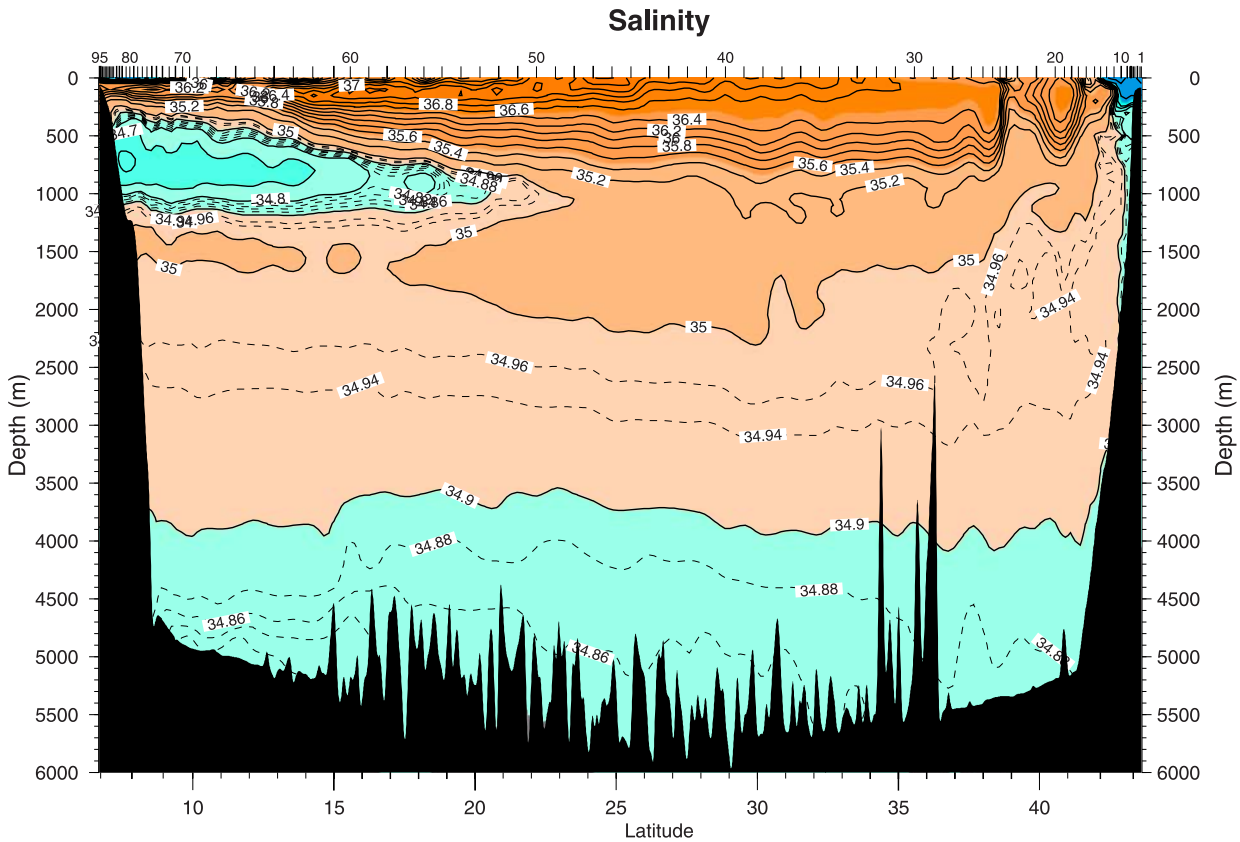

Figure 3b. Salinity.

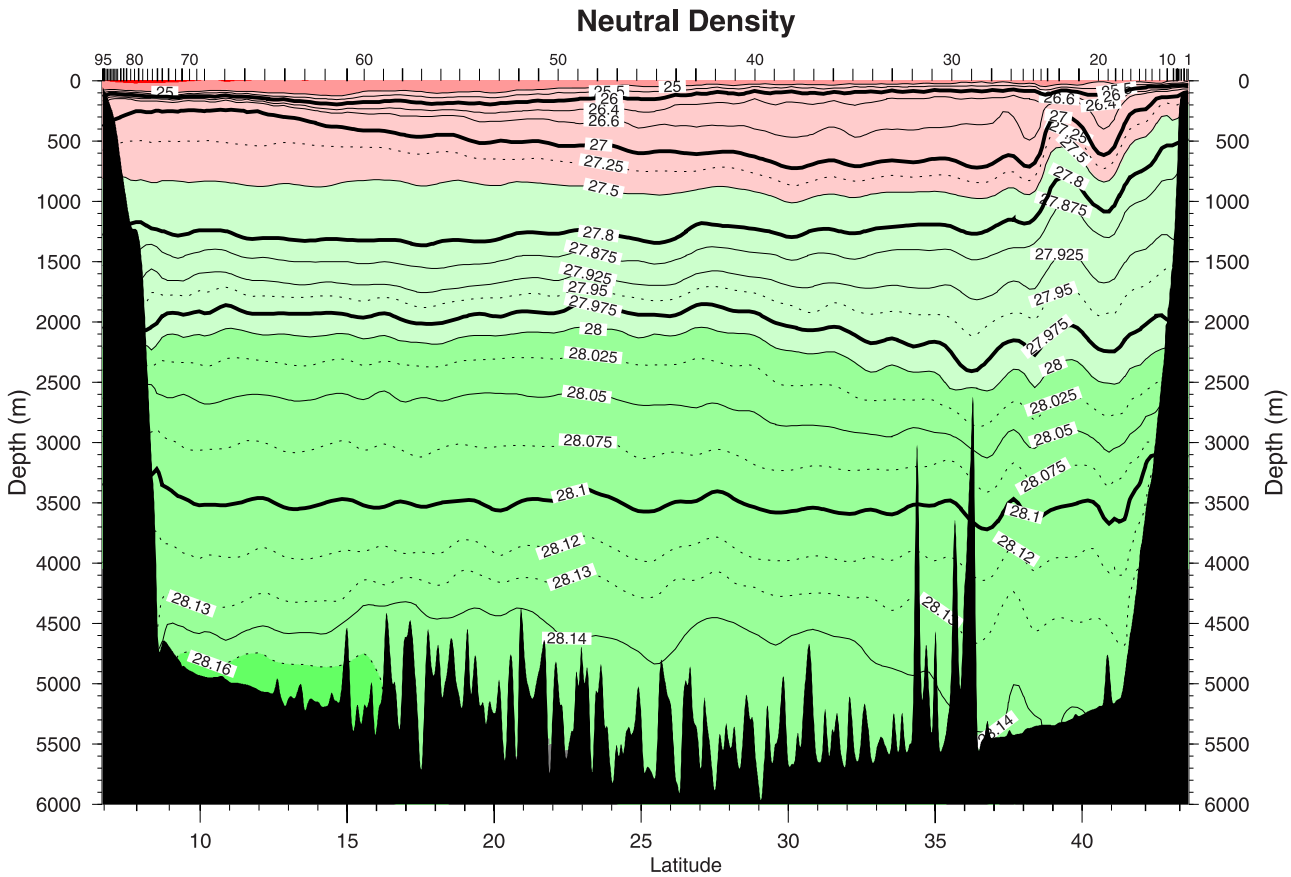

Figure 3c. Neutral density. Solid contours indicate the 17 density layers used in the inverse calculation; bold contours indicate six subsets of the layers referred to in the paper; dashed contours show additional detail.

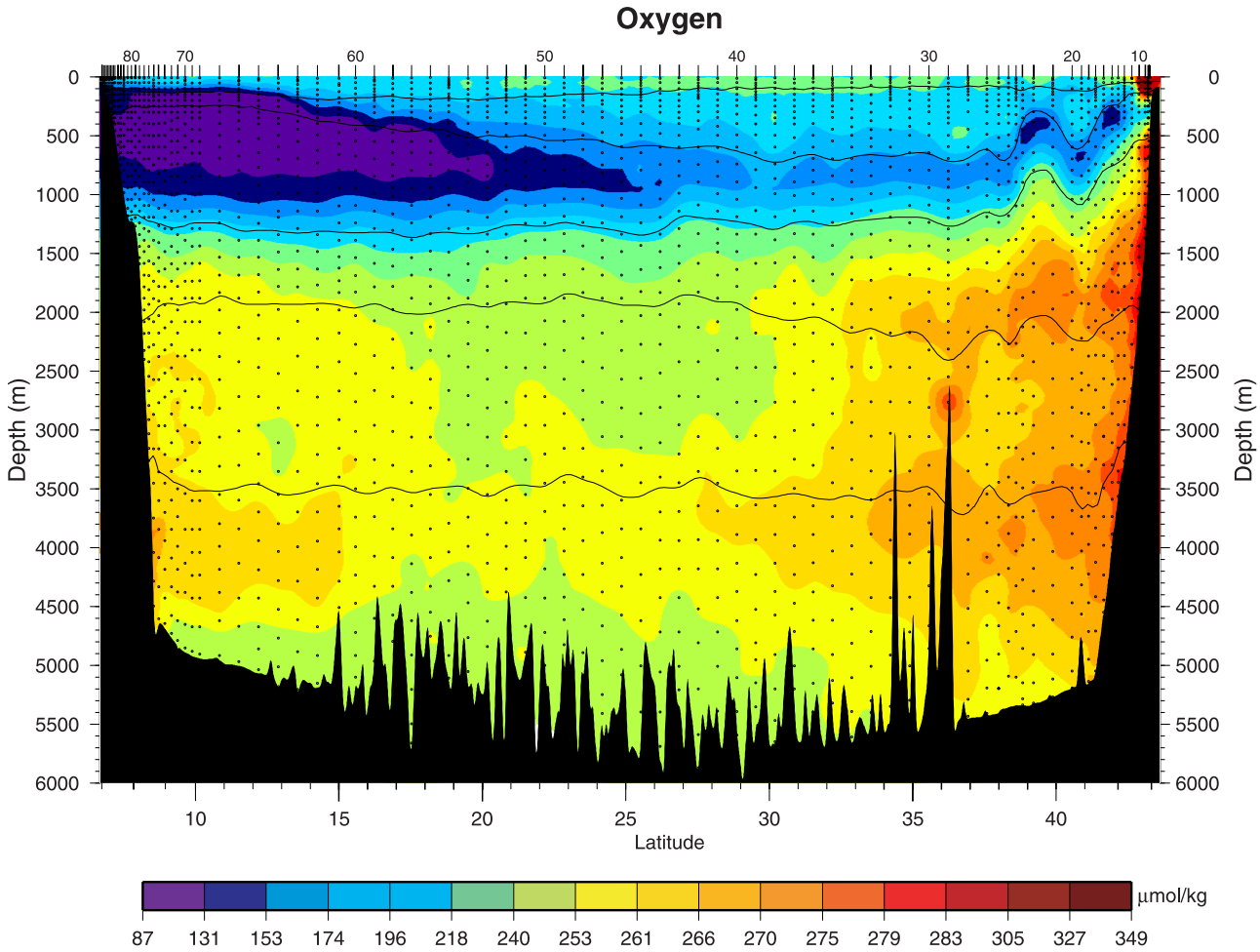

Figure 3d. Dissolved oxygen (μmol kg^{-1}). Dots show where bottle samples were collected. Contours indicate 6 subsets of neutral density layers.

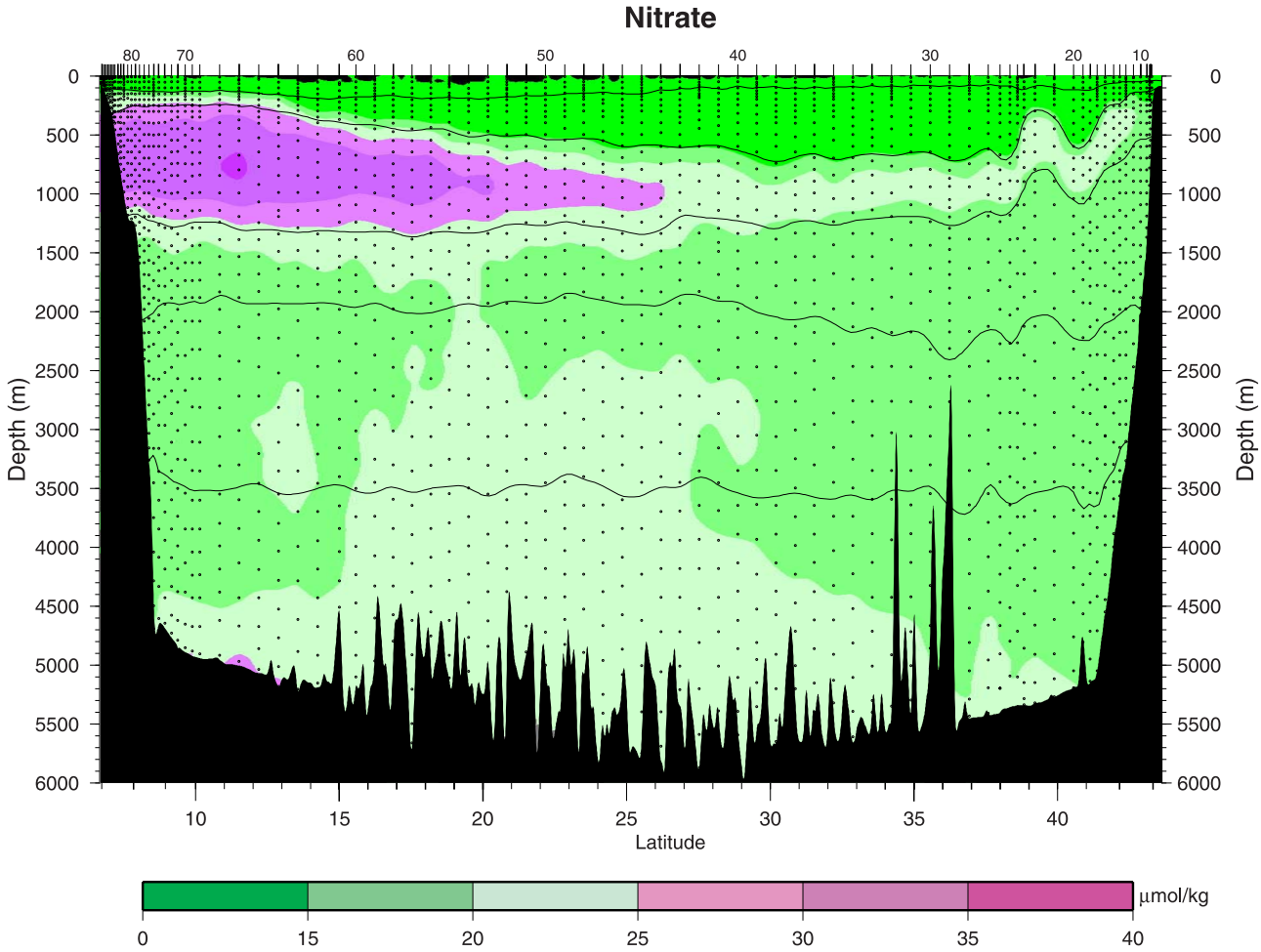

Figure 3e. Nitrate (μmol kg^{-1}). Dots and contours as in Figure 3d.

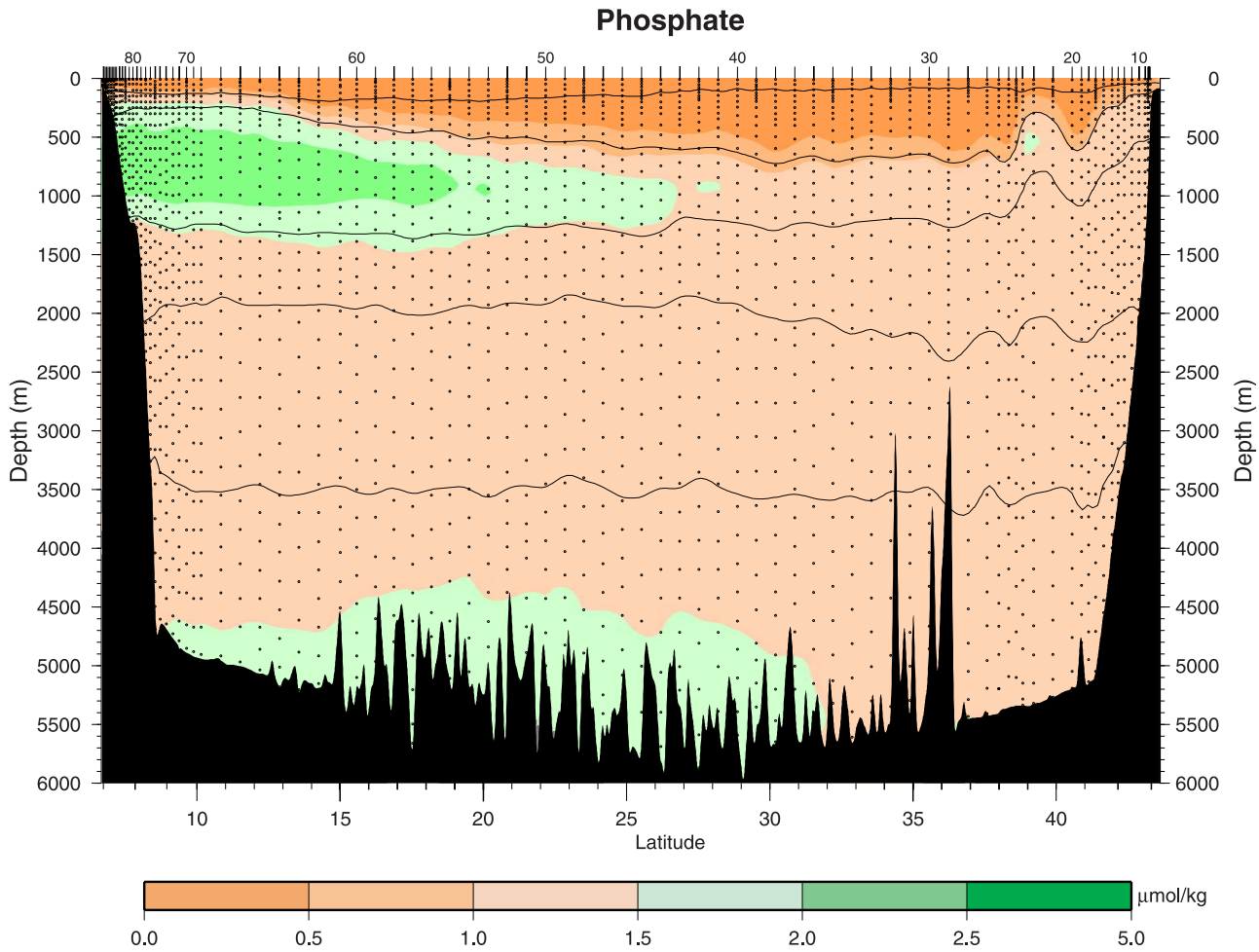

Figure 3f. Phosphate (μmol kg^{-1}). Dots and contours as in Figure 3d.

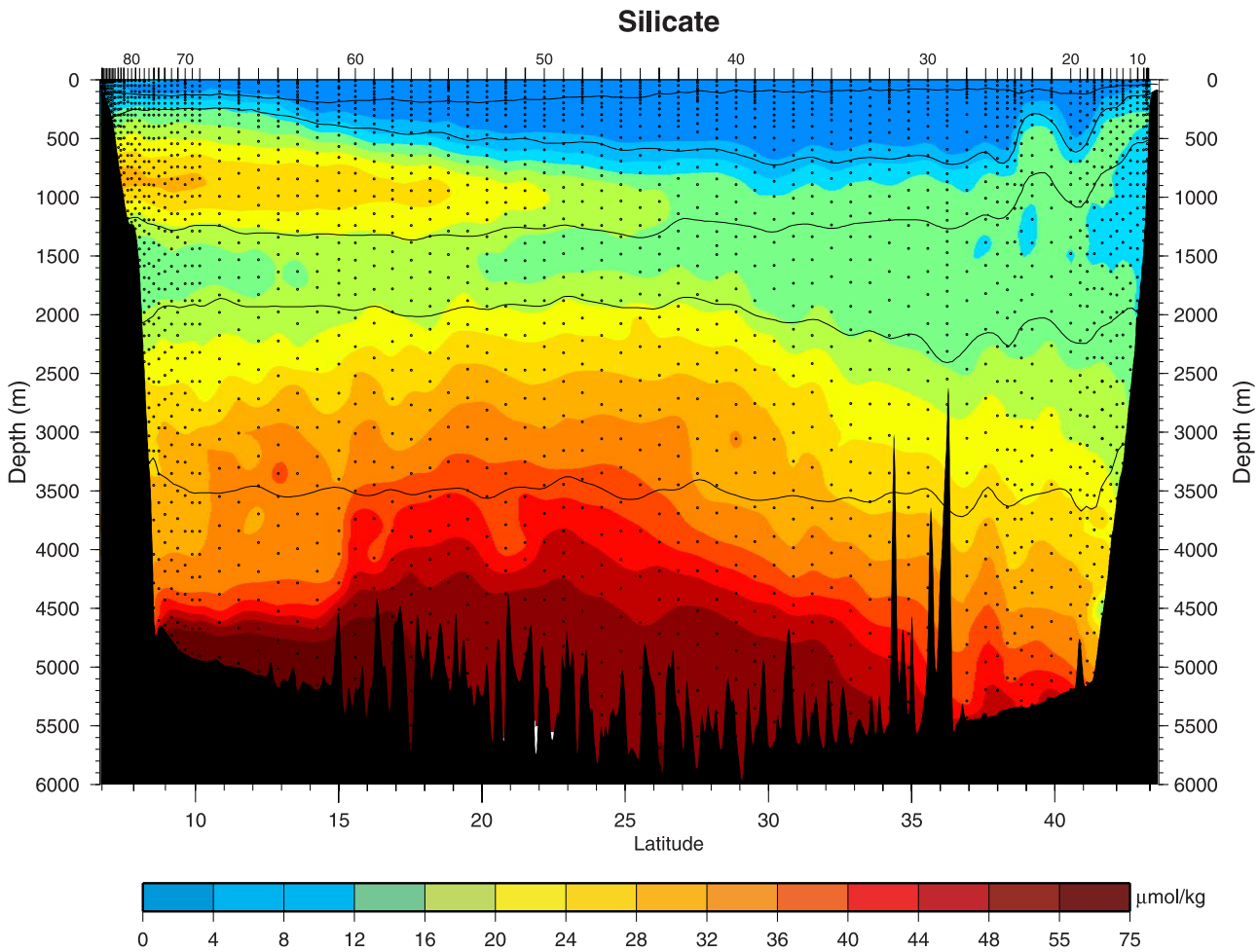

Figure 3g. Silicate (μmol kg^{-1}). Dots and contours as in Figure 3d.

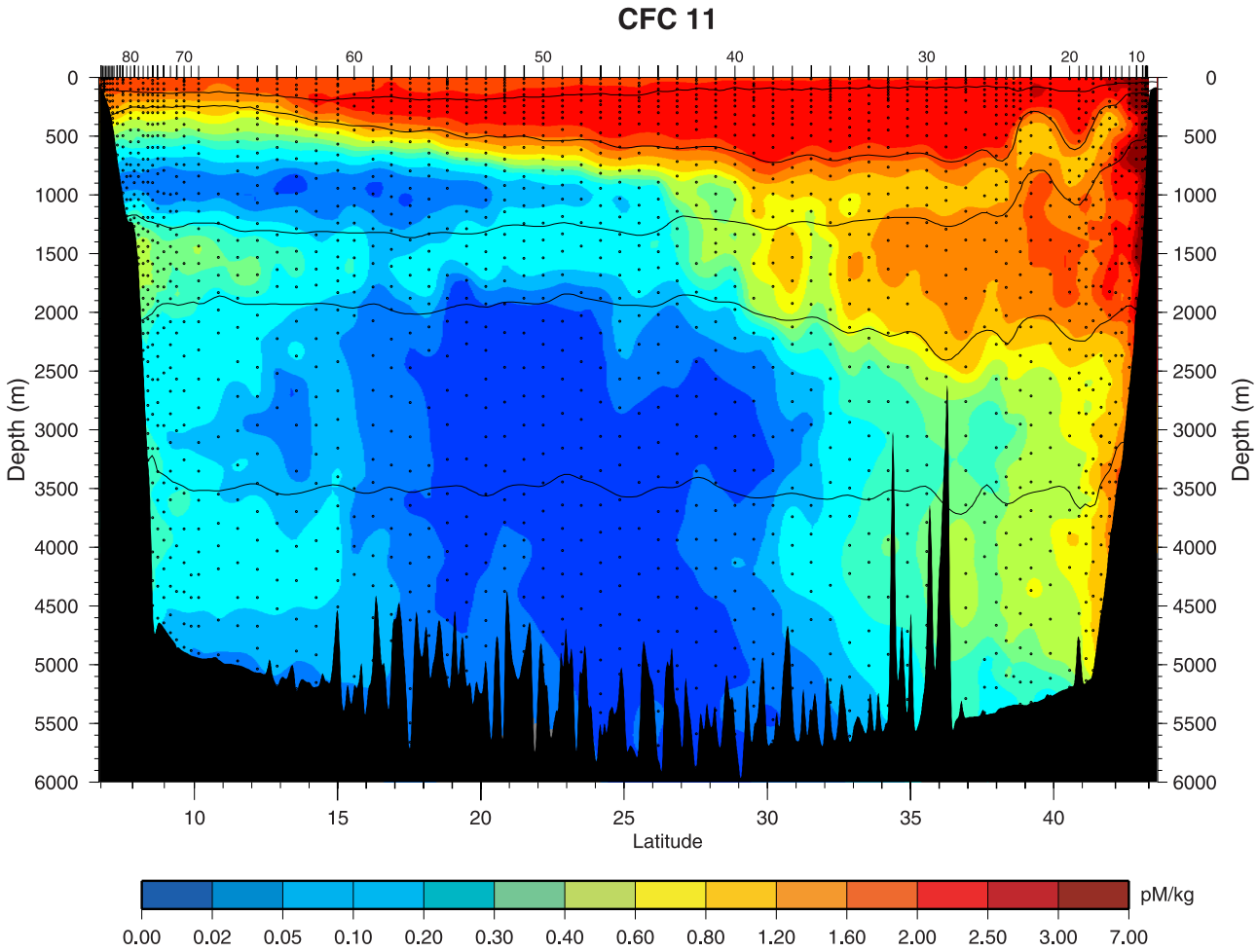

Figure 3h. CFC-11 (pmol kg^{-1}). Dots and contours as in Figure 3d.

addition, the northern end of the section is complicated by the presence of a strong warm-core ring directly south of the slopewater current, north of the Gulf Stream, extending to great depth, and carrying an especially pronounced salinity signal (stations 15–22). According to our velocity calculations (see section 4), the upper part of the ring ($\gamma \leq 27.8$) is recirculating as much as 35 Sv of water. The distribution of dissolved oxygen, especially, but also of CFCs at ~1500–2000 m suggests that the ring may be exchanging water with the westward flowing boundary currents. For example, the relative oxygen maximum at 1800 m at stations 20–21 attains values found, not in the Gulf Stream, but only in the upper DWBC.

[7] The Gulf Stream proper is evident directly south of the ring, in the descent of isopycnals over stations 22–25. The abrupt recovery and second descent of upper thermocline isopycnals, immediately to the south of station 25, is only a surface feature in the velocity, limited to 800 m depth. There is a tight recirculation of the deep water south of the Gulf Stream, visible in the relative maximum in CFC-11 centered around 4200 m (station 28), which appears to be topographically limited, though this may be an artifact of our having taken station 29 directly on top of an uncharted seamount. The isolated oxygen maximum over the seamount arises from a single bottle sample, so we are dubious of its significance. Extending in a narrowing wedge southward from the Gulf Stream lies the subtropical mode water (STMW) of the North Atlantic, the so-called Eighteen Degree Water, formed by late-winter convection south of the Gulf Stream each year, and subsequently advected throughout the subtropical gyre. In our section, the STMW lies at neutral densities γ = 26.4–26.6, with a maximum thickness of about 360 m at stations 25–26, gradually decreasing until, at station 45, the pycnostad becomes indistinguishable from the background gradient. Calculating potential vorticity in this layer as $\frac{f}{\rho_0}\frac{\Delta\rho}{h}$, where f is the local value of the Coriolis parameter, ρ_0 = 1027 kg m^{-3}, $\Delta\rho$ = 0.2 kg m^{-3}, and h is the thickness of the layer bounded by γ = 26.4 and 26.6, we find a mean of 5.9 × 10^{-11}m^{-1}s^{-1}±a standard deviation of 0.84 × 10^{-11} over stations 24–44. In other words, potential vorticity in this layer is constant within 15% over approximately 12 degrees of latitude for which f decreases by 30%: thinning of the layer compensates the lower value of f, going southward.

[8] The interior of the section away from the boundary current influence, below 2000 dbars, is characterized by very low values of CFC-11, relatively high values of nutrients, and a horizontal relative minimum in oxygen, indicating that this water has not been ventilated recently. This unventilated water (CFC-11 values <0.1 pmol/kg) occupies a much broader latitude range than Joyce et al. found along 66°W: approximately 15°–31°N, as compared to 24°–27°N to the west. Centered near 1500 m at 31°N lies an isolated patch of water with CFC-11 values exceeding 0.8 pmol/kg, which may be connected with a nearly identical feature observed in the analogous location along 66°W, where the CFC values are even higher; hence, this water appears to be coming from the west, as confirmed by the LADCP measurements (Figure 2). To the south, around 21°N, another patch of apparently ''younger'' water intrudes into the old interior water between about 3500 m and the bottom, with higher CFCs and oxygen, and lower silicates, nitrates and phosphates.

[9] The southern end of the section displays a similarly rich boundary current structure as does the northern end, though the strong shallow currents over the shelf are difficult to detect in the property sections. The distribution of temperature in the deep water is unremarkable except for the appearance of water colder than 1.4°C: this is Antarctic Bottom Water (AABW), the coldest (and densest) water appearing in our section. This water is also fresher (by 0.02–0.04), lower in oxygen, and higher in silicate, nitrate, and phosphate (Figures 3b, 3d–3g) than the overlying water mass, which consists of North Atlantic Deep Water (NADW) that originates with the Denmark Straits and Iceland-Scotland overflows. The abrupt disappearance of this water mass near 16°N may be associated with the presence of Researcher Ridge just to the east (see Figure 1), with depths shallower than 3000 m. In addition, elevated silicate levels in the NADW below 3500 m depth (seen as the uplift of isolines of silicate in Figure 3g) probably reflect enhanced mixing of AABW into NADW owing to the proximity of the underlying rough topography [*Mauritzen et al.*, 2002]. Overlying the AABW, the rise of deep isotherms (and isopycnals) toward the boundary indicates the presence of the southeastward flowing DWBC. Elevated levels of both oxygen (Figure 3d) and CFC-11 (Figure 3h) extend northward from the boundary as far as 15°N; CFCs are enhanced at two levels (centered at 3700 and 1700 m), while oxygen is enhanced only at the deeper of these levels. We will return to this feature in section 5.3, after calculation of the final velocity section.

[10] At intermediate depths, Antarctic Intermediate Water (AAIW) is prominently visible as a wedge of fresher water extending northward from the southern boundary, centered at about 800 m depth. Like the other southern source water (AABW), AAIW also has higher levels of nutrients. CFCs have entered the deep ocean from the atmosphere in the high latitude deepwater formation regions in both hemispheres. CFCs in both AAIW and AABW are somewhat lower than in surrounding waters because these water masses are farther from their source regions than the surrounding North Atlantic waters. The very high CFC values found in the deep northern boundary current regime had not reached the southern end of our section at the time of the cruise, so the contrast between lower NADW and AABW is weaker at the southern end of the section. In the LADCP currents (Figure 2), the southern DWBC can be seen in the narrow band of strong eastward velocities hugging the continental rise, with maxima centered at about 1500 m, 2300 m, and 3500 m. In contrast, the waters above roughly 800 m depth are flowing westward with speeds up to 45 cm s^{-1} as measured by the SADCP (not shown).

[11] Just below STMW in the north and overlying the core of AAIW in the south lie the most oxygen-poor waters of the section (Figure 3d). In the north, a corresponding relative vertical minimum in CFCs is found, but in the south, the lack of CFCs in southern source AAIW leads to a CFC minimum at intermediate water levels instead of coincident with the oxygen minimum. The low oxygen levels are the combined result of this layer being less ventilated than the waters above and below (especially in the north), while still being subject to oxygen utilization, as

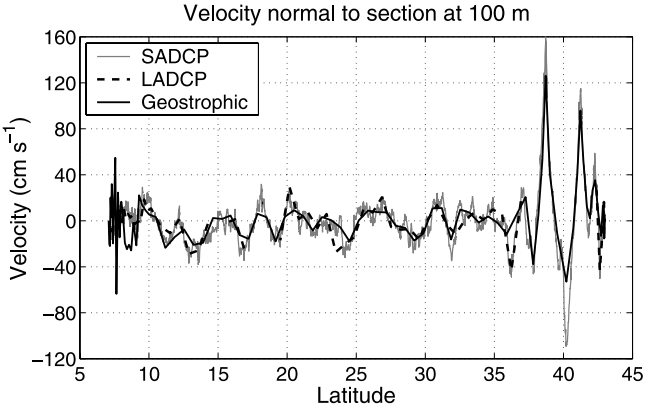

Figure 4. Comparison of velocity normal to cruise track at a depth of 100 m: shipboard ADCP (gray line); lowered ADCP (dashed black line); and geostrophic relative to 2000 dbar (solid black line).

evidenced by the high nitrate and phosphate levels in this same regime (Figures 3e and 3f).

3. ADCP Velocities

[12] For stations 6 through 91, a 150 kHz RDI lowered acoustic Doppler current profiler (LADCP) was mounted on the rosette frame, to directly measure vertical shear of the horizontal velocity throughout the water column, concurrent with the CTD cast. Absolute velocity was then estimated using start and end positions from shipboard GPS navigation data collected during the cast [*Fischer and Visbeck*, 1993]. Unfortunately, owing to instrument problems, a large gap exists in the section of LADCP data. In particular, absolute current profiles are lacking for stations 12 through 27 inclusive, as well as for stations 55, 57 and 61. The early gap extends across the region of strong flow that includes much of the DWBC, the warm core ring, and the Gulf Stream (Figure 2). Although we have used the remaining profiles to select reference level velocities for the geostrophically calculated shear profiles, we note that the comparison between LADCP and CTD velocity shear is expected to be noisy a priori. That is so because the LADCP profiles include ageostrophic components of velocity, and further because the LADCP measures on different spatial scales than CTD-derived velocities, which average the current over the distance between stations. We averaged the LADCP data from adjacent stations for comparison with the geostrophic velocity calculated from the corresponding station pair.

[13] Shipboard ADCP (SADCP) velocity data was also collected along the cruise track, using a 150-kHz narrowband RDI ADCP. Data was collected using DAS248 data acquisition software, in 5-min sampling intervals and 8 m bin sizes. Data were combined with GPS and Ashtech directional data to obtain estimates of absolute flow in the upper 300 to 500 m. Owing to the gaps in LADCP coverage over critical portions of the section, we also used the SADCP velocities to reference the geostrophic shear profiles. Two different averages were considered. First, we computed on-station profiles as the average of all the 5-min profiles collected while the ship was on-station; pairs of on-station profiles were then averaged to obtain a velocity representative of the midpoint between stations, for comparison with the geostrophic shear. Alternatively, we computed the between-station profile as the average of all the 5-min profiles collected while the ship was steaming between stations. Usually these two estimates agreed very closely, but in certain regions of strong horizontal shear (e.g., in the warm core ring and the Gulf Stream proper) they disagreed. Most of these cases occurred in regions lacking LADCP data, so it was important to study the horizontal structure of the velocity as revealed by the full suite of SADCP measurements before deciding which average would provide a better reference for the geostrophic velocity. At station pairs where both LADCP and SADCP data were available, naturally the SADCP profiles calculated by the first method better matched the comparable LADCP velocity profiles.

[14] The three different measurements of velocity (LADCP, SADCP, and geostrophic) show very good agreement across the length of the section. Figure 4 shows the velocity component normal to the cruise track at a depth of 100 m along the entire section, where the geostrophic estimate is relative to 2000 dbars. The SADCP has the best horizontal resolution, but the other two measurements generally reproduce the same horizontal structure, slightly more smoothed out. This result gives us confidence that it is reasonable to reference the geostrophic shear profiles to the directly measured velocities. The notable exception to the good agreement occurs at the far southern boundary, where geostrophic shear generally exceeded ADCP shear; but the choice of reference velocity for these shallow stations does not have a critical impact on the mass budgets for the section because of the small areas involved for these stations.

[15] In order to combine the ADCP velocity information with the geostrophic shear, the hydrographic data were first used to calculate geostrophic shears relative to a pressure of 2000 dbars, or the bottom where the pressure was less than that; below the deepest common level of the two CTD stations, velocity was held constant (for purposes of computing mass transport, the areas of bottom triangles were computed using observed bathymetry between stations). Next, this shear profile was compared with the ADCP shears: ideally, the reference level velocity would be calculated as the mean difference between the LADCP and geostrophic velocity profiles over their common depth range. Realistically, a certain amount of subjectivity was necessary in choosing this reference level velocity. Typically, SADCP and LADCP shears agreed in their region of overlap (the upper few hundred meters), but the absolute velocities were offset by a constant. LADCP velocities for these cases were then shifted by a constant to fit the SADCP velocity, for the following reason. Calculation of absolute velocity profiles from the ADCP depends on navigational data. In the case of the LADCP, only two fixes are used, the ship's position at the beginning and the end of the cast. In the case of the SADCP, navigational data is incorporated into every 5-min average profile, and many of these profiles are averaged over the duration of the station. Thus the SADCP velocity is expected to have a higher signal to noise ratio and therefore be more accurate than the LADCP velocity. We refer to the shifted

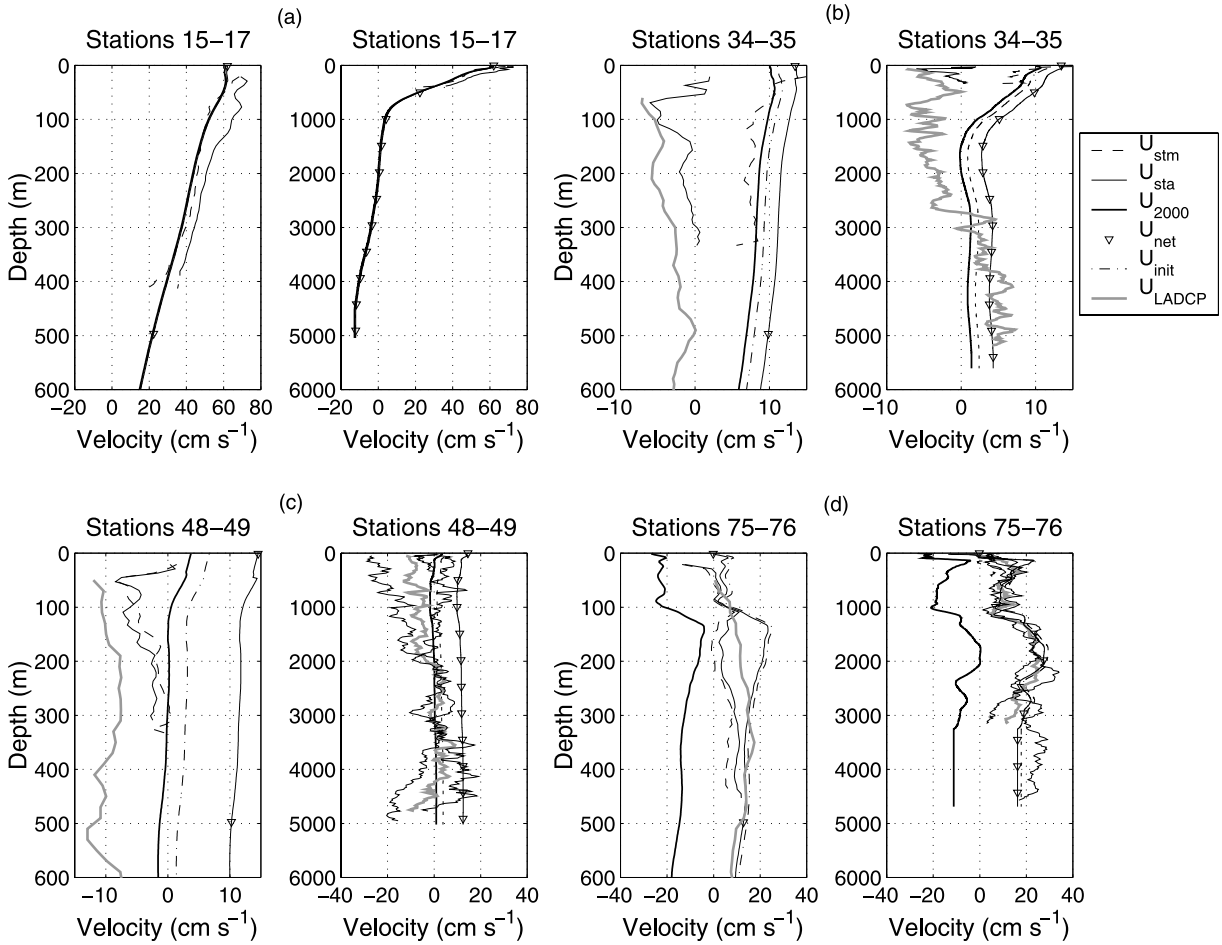

Figure 5. Comparison of different velocity estimates, as a function of depth, for four different station pairs. In each pair of panels the full depth profiles are shown to the right and an expanded view of the top 600 m is shown to the left. Three geostrophic profiles are shown: relative to 2000 dbar (U_{2000}, heavy solid line), referenced to ADCP velocities (U_{init}, light dash-dotted line), and including final adjustment (U_{net}, inverted triangles). Two profiles are shown for shipboard ADCP, using first method (U_{sta}, light solid line) or second method (U_{stm}, light dashed line); see text. Where applicable, the gray solid profile is the LADCP velocity (U_{LADCP}) averaged between the two stations in the pair (uncorrected; see text). The right panels of Figures 5c and 5d also show the individual LADCP profiles comprising the station pair mean.

profiles as the corrected LADCP velocity. Furthermore, geostrophic shear rarely lined up exactly with ADCP shear, for reasons mentioned above; nevertheless, there was usually qualitative agreement between the character of the geostrophic shear and that of the ADCP shears. Then the reference level velocity could be calculated as the average difference between the 2000-dbar referenced geostrophic shear and (if it was available) the corrected LADCP velocity, or to the SADCP velocity where the former was unavailable. For a few profiles, geostrophic and ADCP shears seemed to resemble each other only over a limited part of the water column, in which case a subjective choice was made for the depth range over which to compute the average difference.

[16] Several examples serve to illustrate the different situations encountered in choosing a reference level velocity. In Figures 5a–5d, the heavy solid line is geostrophic velocity relative to 2000 dbars, and the light dash-dotted line is geostrophic velocity referenced to the ADCP. The light solid and dashed profiles are the SADCP velocity computed using the first and second methods, respectively. The gray solid profile (where applicable) is the uncorrected LADCP velocity, and the inverted triangle profile is the velocity after inversion (see section 4). On the left is an expanded version of the full-depth profiles for the upper 600 m, in order to see the details of the SADCP profiles.

[17] Figure 5a shows a case that occurs near the northern end of the section, in the eastward branch of the warm core ring and overlying the DWBC; LADCP data are unavailable. The two estimates of SADCP velocity differ by about 0.08 m s^{-1}, because this is a region of strong horizontal shear; but the vertical shears are similar and match that of the geostrophic velocity (which has been referenced to the between-station SADCP velocity). However, while the upper water col-

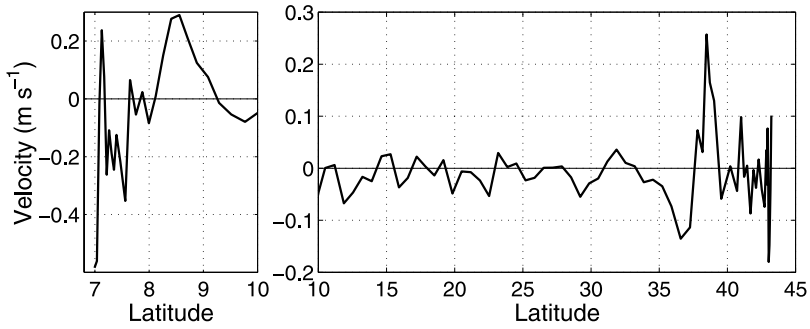

Figure 6. Initial velocity adjustment made to 2000 dbar-referenced geostrophic velocity, as determined by comparison to ADCP. The southern end of the section is expanded and has a different scale for the vertical axis because some reference velocities there are much larger.

umn is dominated by the eastward flow of the warm core ring, the deeper part lies in the strong part of the DWBC (Figure 5a, right). Thus while it is possible to reference the geostrophic profile to the SADCP absolute velocities, it clearly would have been preferable to have absolute velocity throughout the water column, since the deep shear is strong. Figure 5d shows just such a case, in the upper part of the southern DWBC: the correspondence between the LADCP and geostrophic shears is striking, and an initial choice of reference velocity for this station pair is large (over 0.20 m s^{-1}). The two deep, light profiles are the individual LADCP profiles at stations 75 and 76 that were averaged over their common depth range to obtain the midstation profile. Note that holding the geostrophic velocity constant below the DCL gives a strong deep velocity, which is in agreement with the deeper of the two on-station LADCP profiles.

[18] Figure 5b displays a case that occurs near 32.5°N, in an eastward flow well south of the Gulf Stream recirculation. In the upper part of the water column, horizontal shear is relatively strong, with the velocity reversing sign every couple of degrees of latitude (Figure 2): here, as in the case shown in Figure 5a, the steaming version better matches the geostrophic shear in the upper few hundred meters. However, in the deep water, the geostrophic and LADCP shear agree qualitatively, if not in magnitude, and so the reference velocity has been based on comparison with the LADCP, while the LADCP was corrected to the on-station SADCP profile, which it matches well. In Figure 5c, the two estimates of SADCP velocity match well, while the LADCP profile appears to underestimate the velocity by about 0.05 m s^{-1} (based on comparison with the SADCP), and this is taken into account when calculating the reference velocity for the geostrophic profile. We show this example because the final velocity for this station pair, after the inverse, turns out to be even more strongly eastward (compare the solid geostrophic profile with the inverted triangles). The resulting strong eastward deep flow is in agreement with the individual LADCP profile for station 48, shown as the lightweight solid profile in Figure 5c, and also visible between 3500 and 4700 m near 23.5°N in Figure 2. The initial reference level velocity added to the geostrophic shear, based on comparisons with ADCP, is shown versus latitude (see Figure 6): away from the boundary currents and Gulf Stream system, it is generally less than 0.05 m s^{-1}.

4. Inverse Calculations

[19] Our section extends from the Grand Banks of Newfoundland in the north to the coast of Suriname in the south. To the west, the North Atlantic and Caribbean Sea are completely enclosed except for negligible mass flux through the Panama Canal. Hence, to conserve mass within the closed portion, any mass flowing westward across 52°W

Table 1. Layer Definitions

γ_n	Layer	Water Mass
18		
	1	surface layer
25		
	2	upper thermocline
25.5		
	3	SUW
26		
	4	upper thermocline
26.4		
	5	STMW
26.6		
	6	lower thermocline
27		
	7	AAIW
27.5		
	8	AAIW
27.7		
	9	AAIW
27.8		
	10	ULSW
27.875		
	11	LSW
27.925		
	12	CLSW
27.975		
	13	ISOW
28		
	14	ISOW
28.05		
	15	DSOW
28.1		
	16	LDW
28.14		
	17	AABW
29		

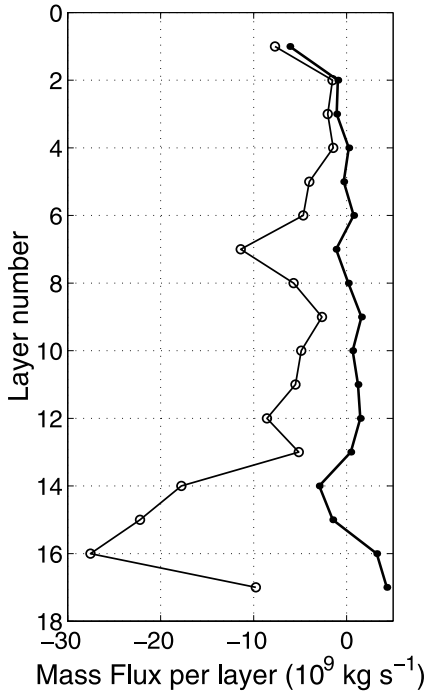

Figure 7. Total mass flux across 52°W section, for each of 17 neutral density layers, for geostrophic velocity referenced to ADCP data (open circles); for geostrophic velocity referenced to ADCP data, and then adjusted by a constant velocity to balance overall mass (solid dots).

must be compensated by an equal flow eastward, or out of the closed volume. The velocity field calculated in the previous section, that is, geostrophic velocity relative to 2000 dbars plus a reference level velocity from comparison with ADCP shear, does not satisfy this constraint: integrating mass transport along the entire section yields a net westward flow across the line of over 140 Sv. (This is equivalent to an average velocity over the section of less than 0.7 cm s^{-1}. To some degree, the transport imbalance is an indicator of the errors involved when making subjective choices in the referencing scheme. A comparable imbalance was found by *Donohue and Toole* [2003] for a near-synoptic survey in the southwest Indian Ocean.) Furthermore, we expect mass to be conserved in density layers not subject to buoyancy forcing. Following *Joyce et al.* [2001], we divided the water column into 17 neutral density layers roughly corresponding to water masses (Table 1), and we seek a velocity field such that mass is nearly conserved in each of these layers, as well as overall for the section. This is tantamount to claiming that no conversion of water from one density class to another occurs in the volume west of the section in excess of a prescribed a priori error (see below). (Of course, conversion between layers does indeed occur, most notably in the creation of 18 Degree Water south of the Gulf Stream, due to late-winter convection. Unfortunately, we cannot specify actual rates of conversion a priori because they are not well-known enough.) Even if we add the uniform velocity to the entire section as suggested above, imbalances of up to 4 Sv remain in the mass transports of individual layers, especially at depth. For reference, meridionally integrated mass flux as a function of density layer, computed from the velocities calculated in section 3 as well as using a uniform velocity to balance overall mass transport, is shown in Figure 7.

[20] Additional adjustments are required in order to obtain a more realistic velocity field, though ideally such adjustments should not swamp those made initially to match the ADCP velocities. In order to achieve this end, we have applied an inverse model, following *Joyce et al.* [2001]: the details of the model are discussed therein and will not be repeated in their entirety here. The inverse is constructed using the constraints stated above, that integrated mass transport along the entire section be conserved within each of the 17 layers as well as overall. Initially, mass transports for each layer and each station pair were calculated using the velocity field referenced to the ADCP data as described in section 3. At this stage, we also have included the Ekman transports across 52°W due to the meridional component of the wind stress, using estimates from the NSCAT/ERS-1 for the period 1991–1998 [*World Ocean Circulation Experiment* (*WOCE*), 1998]. These transports are westward south of 26.5°N and eastward north of there, with magnitudes of −1.2 and 0.3 Sv, respectively, and it is assumed that they are confined to the uppermost density layer.

[21] What we seek is a 93-element vector comprised, in this case, of 93 velocities that constitute additional reference velocity adjustments to be made to the geostrophic velocity profiles for each station pair. The inverse problem thus consists of an underdetermined linear system with 18 equations, corresponding to the mass conservation constraints, and 93 unknowns, which was solved using the Gauss-Markov method [*Wunsch*, 1996]. This method requires a preliminary variance for each constraint as well as each element of the solution vector. Recognizing that

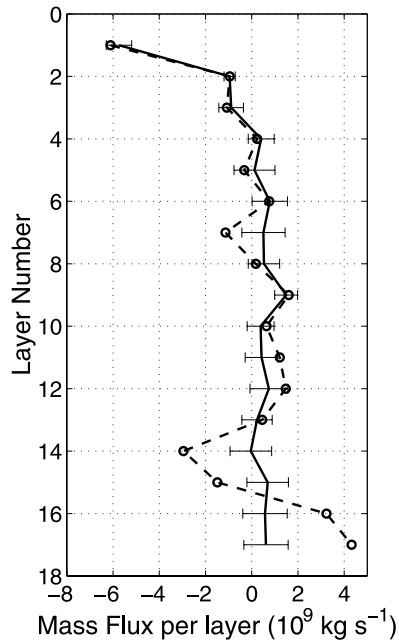

Figure 8. As in Figure 7. Dashed line is the same solution as solid dots shown in Figure 7; solid line is for solution resulting from inverse that imposes mass conservation in individual layers. Errors due to inversion are shown for the latter solution.

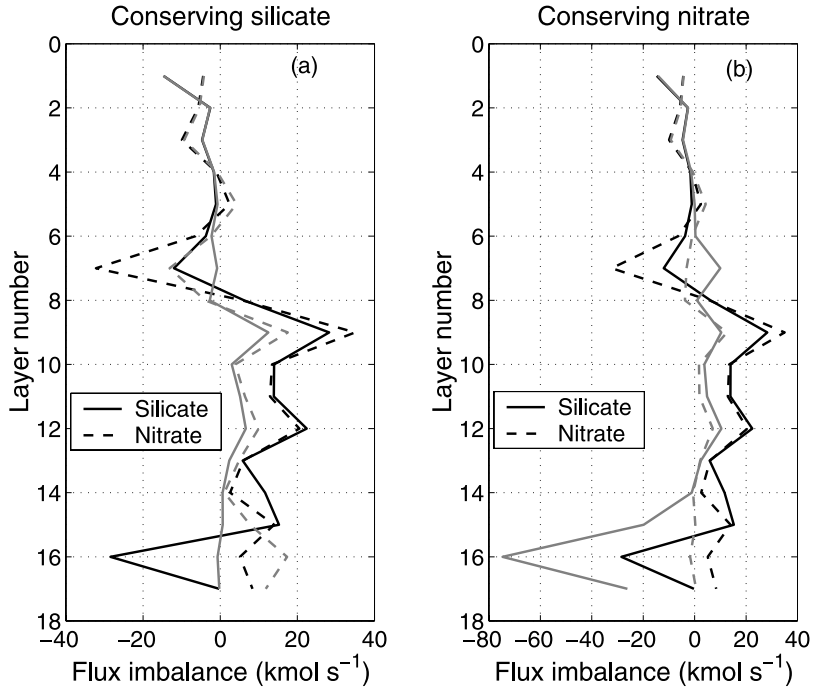

Figure 9. Total nutrient flux across 52°W section in each of 17 neutral density layers; solid (dashed) is silicate (nitrate). Black profiles are from inverse solution conserving only mass; gray profiles conserve both mass and either (a) silicate or (b) nitrate. Note different x axis scales.

mass is less likely to be conserved in those layers closest to the surface, we prescribed a tolerance for the mass imbalance of 2 Sv in the top 4 layers (neutral density less than 26.4) and of 1 Sv in the remaining layers. For the section as a whole, mass is expected to be conserved more closely (the only deviations from perfect conservation should be due to evaporation, precipitation and river runoff), so the tolerance for the overall mass balance is just 0.5 Sv.

[22] As noted above, we would also like to minimize the deviation of the final velocity profiles from their starting point based on the direct velocity measurements; indeed, the inverse requires us to prescribe a priori the variance of the vector of additional reference velocity adjustments. For the 66°W section, *Joyce et al.* [2001] had better LADCP coverage, and they were able to specify a velocity variance of $(0.05\ \mathrm{m\ s^{-1}})^2$ for all stations but a very few lacking LADCP velocities. Along 52°W, the lack of LADCP coverage was much greater, and spanned the region of strong flows in the north, suggesting that a larger tolerance was more appropriate; some experimentation with different tolerances led to a final a priori choice of $(0.10\ \mathrm{m\ s^{-1}})^2$ for the velocity variance in the model, for all stations. After incorporating the new reference velocities, yielded by the inverse, into the initial field, we recalculated the mass fluxes: Figure 8 shows the meridionally integrated mass flux as a function of density layer for this new velocity field, along with mass flux from the (balanced) ADCP-adjusted solution. The negative values of mass transport in the top three layers of the section indicate that more water is flowing westward across 52°W in these layers than re-crosses the meridian flowing eastward. This is a sensible result, since we would expect there to be some conversion of light (warm) water to denser water both in the northern parts of the western basin as well as south of the Gulf Stream in winter. This loss is balanced by smaller increases (generally less than a Sverdrup) in the remaining layers. Initializing the inverse with the ADCP-referenced velocity field that is adjusted to balance mass overall (Figure 7) yields a solution that is virtually indistinguishable from the one presented here.

[23] We also calculated the salt and nutrient transports in each layer: Figure 9 shows the meridionally integrated transports of silicate (solid black line) and nitrate (dashed black line) for this new velocity field. Notice that while mass imbalances have been reduced to less than a Sv in most layers, relatively large imbalances remain in both the silicate and nitrate fluxes. These flux imbalances track one another throughout most of the 17 layers, and thus contain more or less the same information for imposing further constraints on the inverse: hence, we choose to impose constraints involving just one of these properties. It is straightforward to include a set of constraints on property fluxes analogous to those already included for mass fluxes, and so we imposed such constraints, in turn, on either silicate or nitrate, choosing a priori variances that parallel those used for the allowed mass imbalances in each layer and overall. We found that adding silicate conservation to the inverse also reduces nitrate imbalances in all but layers 5, 16, and 17; in these layers the increases are modest, and the new imbalances are reasonable (Figure 9a). Likewise, when nitrate conservation (but not silicate conservation) is added to the inverse, silicate imbalances are mostly reduced; however, unacceptably large increases occur in layers 16:17 (Figure 9b).

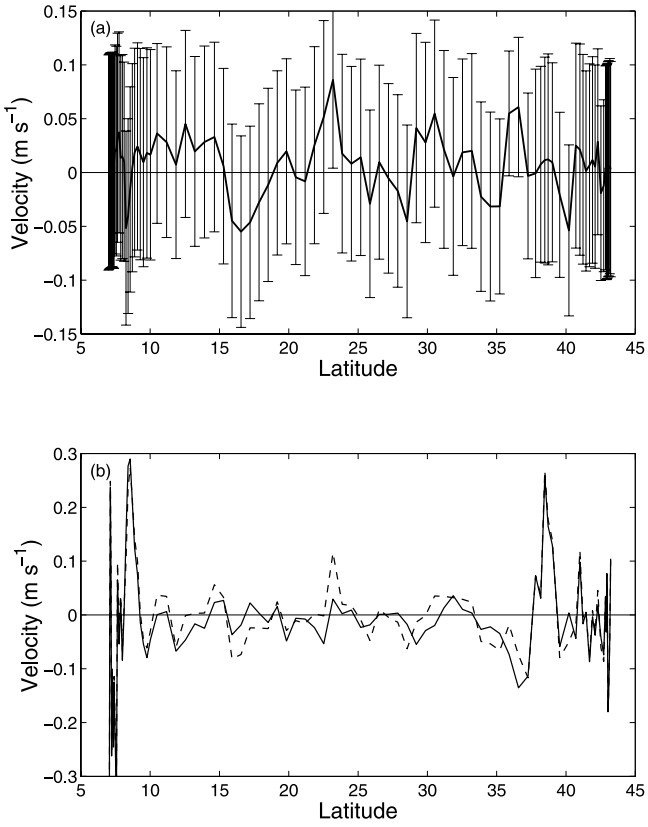

Figure 10. (a) Solution vector for final inverse, with error bars. (b) Initial reference velocity added to 2000-dbar referenced geostrophic velocity field (solid) and net reference velocity added to geostrophic velocity (dashed). The dashed line is the sum of the solid line and the velocity values shown in Figure 10a.

[24] In order to preserve consistency with the 66°W analysis, and owing to the results shown in Figure 9, we choose to include 18 additional constraints based on conserving silicate. The a priori variances assigned to the silicate flux equations parallel those for mass, and are: for layers 1:4, 20 kmol s^{-1}; for layers 5:17, 10 kmol s^{-1}; and overall, 5 kmol s^{-1}. Thus the inverse now has a total of 36 constraints, and it is again applied to the initial velocity field determined in Section 3. The solution vector is a (new) reference velocity adjustment to be added to each station pair (Figure 10a); Figure 10b shows the total barotropic velocity (ADCP + inverse determined) added to each station pair as a function of latitude. Generally, the new adjustments are just a few cm s^{-1}: the standard deviation of the solution vector is 2.5 cm s^{-1}. In cases where the barotropic velocity from the inverse exceeds 4 cm s^{-1}, one of three situations obtains: (1) the final velocity profile may accurately match the deep LADCP from just one of the two stations in the pair; (2) deep LADCP data is missing altogether for one or both of the stations in the average; or (3) the station pair may be in a region of strong flow, such as the Gulf Stream or DWBC.

[25] Figure 11 shows the meridionally integrated mass and silicate fluxes as a function of density layer for the final velocity field, compared with the fluxes for the previous solution conserving mass only. Error bars, shown for the new solution, represent errors due to the inverse only. Note that the vertical distribution of mass flux is changed very little, yet the silicate fluxes are greatly reduced. Evidently, the horizontal distribution of the transports has been altered to achieve silicate conservation. The final velocity field is shown in Figure 12. While the character of the flow field above about 1000 m is very like that in the LADCP velocities (Figure 2), the deep flow for the former is vertically smoothed compared to the LADCP velocities,

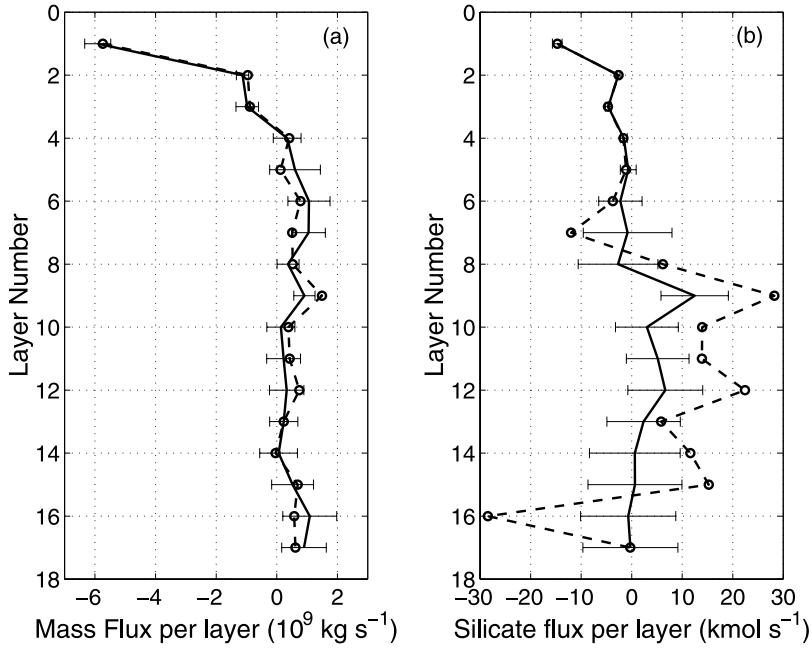

Figure 11. Total (a) mass and (b) silicate fluxes across 52°W section for 17 neutral density layers; dashed profiles are for solution conserving mass only; solid profiles are for solution conserving both mass and silicate. Errors bars are shown for the latter, for errors due to inversion only.

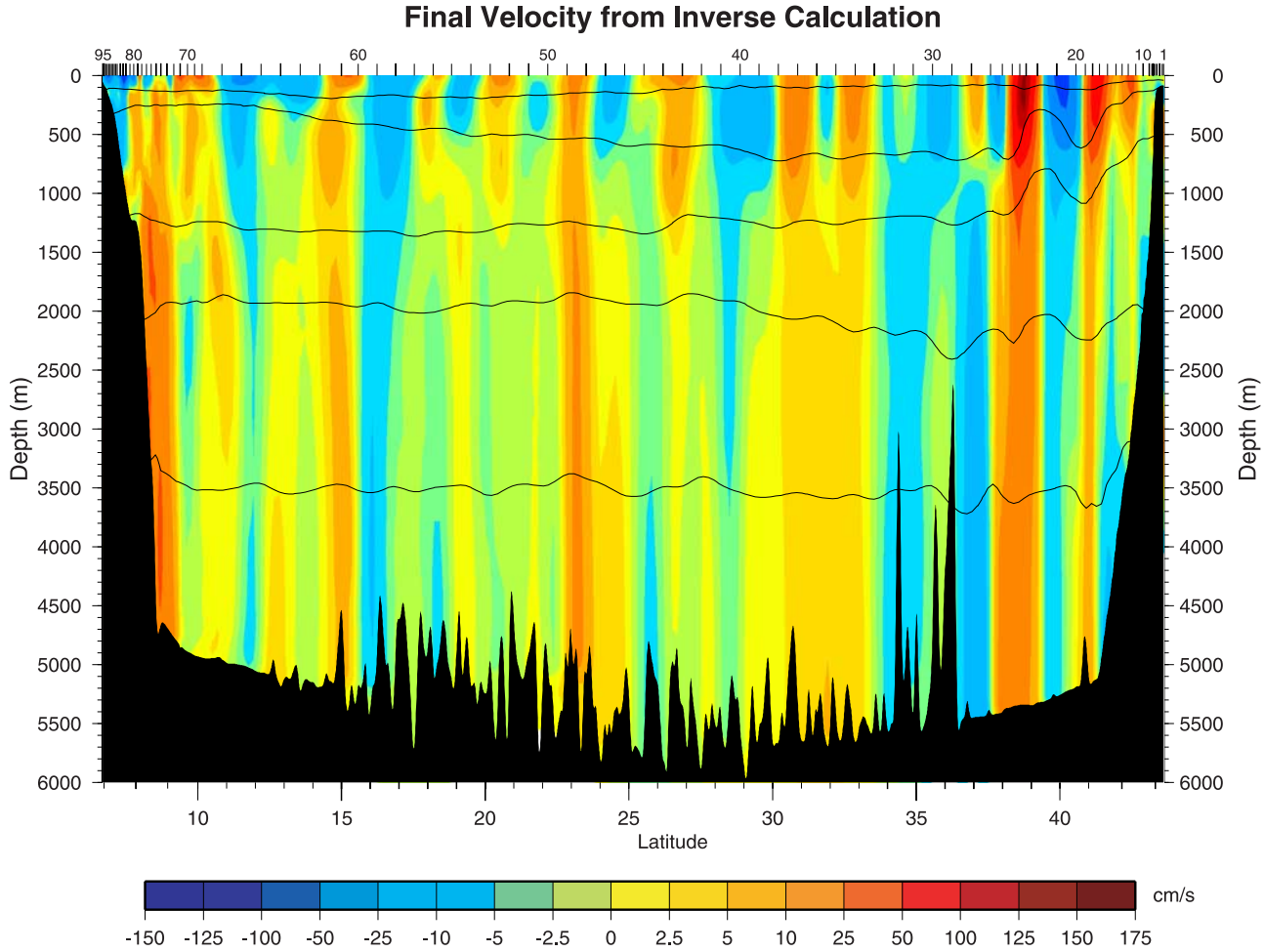

Figure 12. Adjusted geostrophic velocities for 52°W section, after initializing to ADCP data and using inverse model with mass and silicate constraints. Sign convention same as in Figure 2.

since the vertical shear has been calculated using geostrophy.

5. Discussion

[26] One way to readily view the effect that each adjustment to the velocity field has on the circulation is to plot the vertically and meridionally integrated mass transport stream function for each of the velocity fields discussed so far (Figure 13): the 2000-dbar referenced, geostrophic velocity; the geostrophic velocity adjusted to the ADCP values (uniformly adjusted to balance overall volume transport, as well); the solution resulting from conserving mass alone; and the solution resulting when both mass and silicate are conserved. Of course, since there is no reason to expect that 2000 dbars is actually a level of no motion, the biggest change in stream function character occurs due to the ADCP-based adjustments: the Gulf Stream becomes much stronger, and has a southern recirculation. The southern expression of the DWBC also strengthens and becomes vertically coherent (Figure 14), dominating the total stream function south of 10°N. Interior eddies are somewhat more pronounced as well. The inverse solution conserving mass in 17 individual layers, as well as overall, displays not so

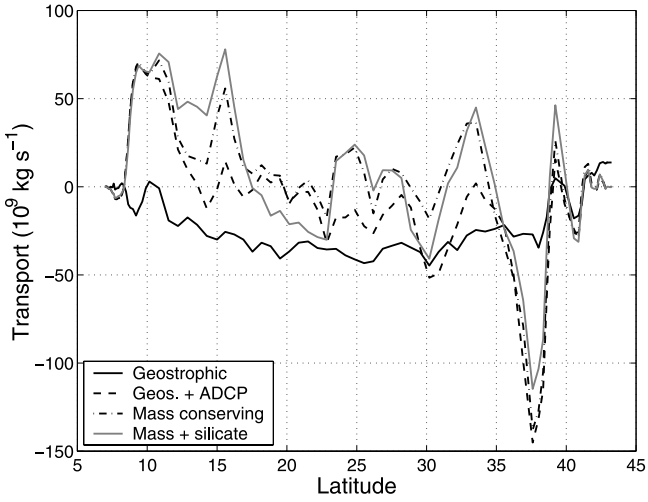

Figure 13. Total mass transport stream functions along 52°W for four different velocity fields discussed in the text. Top to bottom transport is integrated northward from the southernmost station.

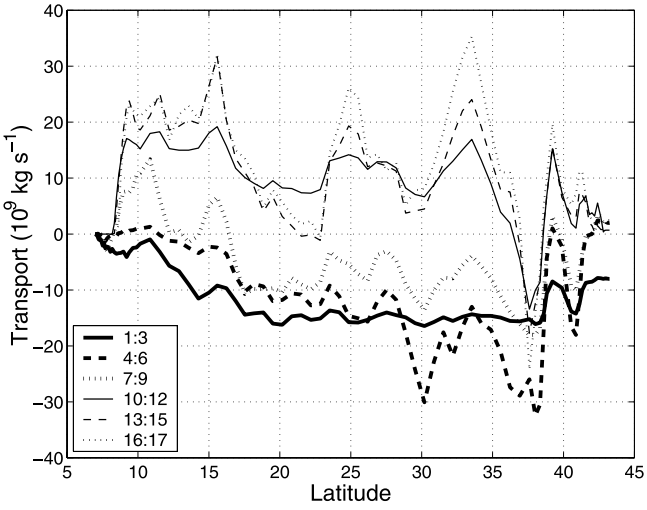

Figure 14. Meridional mass transport stream functions for 6 groups of neutral density layers indicated by the bold contours in Figure 3c. Transport in each layer is integrated northward from the southernmost station.

much a qualitative change as a quantitative one, redistributing the stream function primarily in the interior portions of the line. However, conserving silicate as well as mass leads to a substantial shift of the mass transport stream function south of 20°N: the organized westward flow north of the southern DWBC, which largely occurs between 11°–14°N in the mass conserving solution, shifts northward of 16°N, where water properties differ rather significantly from those south of 15°N. This feature is discussed in more detail later in this section. Table 2 lists transports of the prominent circulation features for the velocity field shown in Figure 12; Figure 14 displays mass transport stream functions, based on this final solution, for 6 subsets of the 17 density layers used in the calculations.

[27] In the uppermost layers, generally westward flow south of 20°N is only partly balanced by eastward flow in the Gulf Stream (Figure 14, layers 1:3); as seen previously, a net conversion of these shallow waters to denser waters must occur west of the section, amounting to 8 Sv. A fourth of this can be accounted for by layers 4:6, which include STMW, and for which generally westward flow south of 25°N is more than compensated by eastward flow in the Gulf Stream. The character of the mass transport stream function for layers 7:9, the intermediate waters, is somewhere between that of the shallow layers and that of the deep waters. At the southern boundary, a small westward flow occurs onshore of the 1200 m isobath, but the intermediate waters flow eastward where they overlie the southern DWBC. This layer appears to be dominated by frequent flow reversals more than by trends in the interior, with the result that 2.3 Sv more exits the volume west of 52°W than enters it. The deep velocity and transport fields (layers 10:17) are generally coherent and are dominated by the boundary currents, the Gulf Stream, and recirculation gyres. These are all discussed in more detail below.

5.1. Northern Boundary Currents

[28] The shallow boundary current systems at both ends of the section are largely dictated by the adjustments made to the geostrophic field from comparison with ADCP velocities: the inverses do not make significant changes in these areas, because in regions of shallow flow, with narrow station spacing, adjustments to velocity would have little effect on the overall mass or silicate transports. Waters flowing along the continental boundary arrive here from the subpolar North Atlantic only after successfully negotiating the Grand Banks of Newfoundland and encountering the North Atlantic Current; it is still a subject of speculation to what extent the subpolar gyre extends westward in the North Atlantic. In the past decade or so, studies of the northern boundary current system at this location have begun to include a number of direct measurements: *Hendry* [1993] collected data from 7 moorings seaward of the 2000 m isobath along 50.15°W from 1988–1990; *Hogg* [2000] deployed an array of 9 moorings with 21 current meters in this region from 1995–1997; and *Pickart and Smethie* [1998] used hydrographic sections combined with acoustic transport float data to examine absolute geostrophic velocities in the DWBC at 55°W.

[29] On the basis of the water property distributions from station 1 to 18 (and particularly the presence of relative highs in CFCs), we conclude that all of the westward flow over the shelf and slope is recently ventilated. Near the shelfbreak and upper slope, the Labrador Current carries 8.6 Sv over the 2000 m isobath, if we include the small flow over the shelf. Of this, 6.0 Sv appears to come directly from the Labrador Sea, where at 56°N the Labrador Current carries some 13.1 Sv southward (*Hall and Pickart* [2003]; hereafter HP03; details may be found at http://www.whoi.edu/science/PO/people/pickartgroup/Online_pubs_main.htm). Farther offshore, water of the same density is contiguous with the DWBC, and carries an additional 4.4 Sv, but HP03 suggest that this is not part of the Labrador Current. For purposes of discussion, we simply include it as part of the shallow DWBC. Seaward of the Labrador Current are two CFC/oxygen maxima, at about 1500 and 2000 m, embedded in the upper part of the DWBC. These are probably the products of Labrador Sea Water (LSW) formation occurring in two different seasons; *Lazier et al.* [2002] show that there is large interannual variability in the hydrographic properties of this water mass. In the deep water, CFC and oxygen extrema occur at 3500 m up against the continental slope, while the velocity core occurs over the 4500–5000 m isobaths (see HP03). The westward flowing transport between stations 12 and 18 below $\gamma = 27.975$ is 16.5 Sv, for a total of 29.5 Sv flowing westward inshore of the warm core ring. However, the work by HP03 indicates that the deepest water, which includes the velocity maximum core, does not come from the subpolar gyre but is more locally recirculated, and includes remnant AABW. We estimate this transport as 8.4 Sv north of the ring (nominally the transport below about $\gamma = 28.1$, but see HP03 for more details). Thus the net westward flow of 29.5 Sv north of the warm core ring comprises 8.6 Sv of Labrador Current flow, 12.5 Sv of DWBC flow, and 8.4 Sv of recirculated deep water. From his 7 moorings, *Hendry* [1993] found a net 17 Sv of deep water flowing westward north of 41°N, but recall that he used data only seaward of the 2000 m isobath, thus possibly missing most of the 8.6 Sv we found onshore of that depth. Hendry did not distinguish between flow coming directly from the Labrador Sea and recirculated water, so this 17 Sv

Table 2. Transports of Major Currents

Feature	Partition	Stations	Latitude Range	Net,[a] Sv
Labrador Current		1–11	42.40/43.25N	−8.6
Slopewater Current	onshore	6–9	42.82/42.97N	1.3
	offshore	11–14	42.40/41.82N	11.2
Deep flow north of WCR	$27.0 < \gamma < 27.975$, DWBC	12–18	41.13/42.19N	−4.4
	$27.975 < \gamma$ 28.1,[b] DWBC			−8.1
	$\gamma > 28.1$,[b] recirculating flow			−8.4
	total			−20.9
Warm core ring	$\gamma < 27.8$	14–22	39.22/41.82N	
	eastward flow	14–19	40.88/41.82N	33.5
	westward flow	19–22	39.22/40.88N	−38.2
Warm core ring	$\gamma > 27.8$	15–22	39.22/41.57N	
	eastward flow	15–20	40.55/41.57N	16.5
	westward flow	19–22	39.22/40.88N	−41.4
Gulf Stream	$\gamma < 27.8$	22–27	37.60/39.22N	62.8
	$\gamma > 27.8$	22–27	37.60/39.22N	105.9
	total			168.7
Gulf Stream southern recirculation	$\gamma < 27.8$	26–29	36.23/38.02N	−10.2[c]
	$\gamma > 27.8$	27–29	36.23/37.60N	−75.7
	total			−86.0
Southern DWBC	$27.8 < \gamma < 27.975$	72–79	8.06/9.20N	17.1
	$27.975 < \gamma < 28.1$	71–78	8.18/9.38N	23.8
	$\gamma > 28.1$	71–76	8.48/9.38N	23.2
	total	71–79	8.06/9.38N	64.1

[a]Nets integrate only over the positive (eastward) OR negative (westward) velocities in the station/lat range.
[b]Here 28.1 is nominal division. See text.
[c]Integrated over both eastward and westward values of surface eddy.

should be compared with the 20.5 Sv we find north of the ring, excluding Labrador Current flow. Between stations 11 and 14, splitting the westward flow, lies the warmer and more saline slopewater current [*Pickart et al.*, 1999], with an eastward transport of 11.2 Sv; the warm and saline anomaly observed around 200–300 m depth farther onshore may well be a part of the jet, and carries an additional 1.3 Sv, for a total transport of 12.5 Sv. The slopewater current is believed to be a northeastward bifurcation of the Gulf Stream [see, e.g., *Fofonoff and Hall*, 1983], whose transport has been estimated as low as 2–3 Sv at 55°W [*Pickart et al.*, 1999] or as high as 10–20 Sv farther west [*McLellan*, 1957; *Fofonoff and Hall*, 1983].

[30] At the time of our cruise, a warm core ring lay between the boundary current waters and the Gulf Stream. The upper part of the ring abuts the slopewater current and partially overrides the DWBC, recirculating 35–36 Sv of water between stations 14 and 22 (Table 2). In the deep water ($\gamma > 27.8$), the eastward flowing arm of the ring reaches to the bottom from stations 17–20, and transports 16.5 Sv. By contrast, the deep westward flow just north of the Gulf Stream, between stations 19 and 22, exceeds 40 Sv: if we suppose that 16.5 Sv of this amount can be attributed to the ring, then an additional 25 Sv remains. Some of this water carries oxygen and CFC signatures that cannot derive from the Gulf Stream but appear to originate in more recently ventilated water; but along constant neutral density surfaces, both the middepth (1500–2000 m) and deep (3500–4000 m) maxima in CFC-11 and oxygen are stronger at stations inshore of the ring. We thus conclude that part of the westward transport in the warm core ring constitutes the far eastern end of the Northern Recirculation Gyre (NRG) of the Gulf Stream [see, e.g., *Hogg et al.*, 1986]. There is some uncertainty regarding the size of the NRG this far east. In their 1986 paper, Hogg et al. estimated that the gyre contributed 20 Sv of recirculating deep flow to the Gulf Stream near 63°W, with the gyre extending between the New England Seamount Chain and the Grand Banks. *Richardson*'s [1985] mean Eulerian view of the circulation along 55°W north of 35°N, compiled from disparate measurements collected over many years, implied northern recirculation of Gulf Stream water with a magnitude of 25–30 Sv. More recently, *Bower and Hogg* [1996] used two years of current meter data along 55°W to deduce a NRG strength at 55°W of 32–42 Sv. Adding the recirculating deep water components both north and south of the ring, we find a total NRG strength of 33–34 Sv, which is in line with these various estimates.

5.2. Gulf Stream System

[31] The Gulf Stream proper lies between stations 22 and 26 above $\gamma = 27.0$, and between stations 22 and 27 below that: thus defined, it transports 169 Sv eastward (63/106 Sv above/below $\gamma = 27.8$). To the south is a broad region of westward flow (Figure 12), not all of which can constitute recirculating Gulf Stream water. The character of the deep transport stream functions, as well as the deep (3500 m) oxygen and CFC fields, indicates that the so-called southern recirculation is limited to the north of station 29. In the shallow water, the small dip and recovery of isotherms just south of the stream represents an eddy-like feature confined to densities $\gamma < 27.0$. We were unable to find any satellite data to further elucidate what this feature might be, and simply include its net transport in the southern recirculation. This yields a westward recirculation of Gulf Stream waters amounting to 86 Sv, or half the total Gulf Stream transport; of this, 76 Sv occurs below $\gamma = 27.8$ (Table 2). Our Gulf Stream transport is somewhat high compared to what might be expected at this longitude. *Hogg* [1992] calculated the synoptic Gulf Stream transport at 55°W from a two-year moored current meter array of 149 Sv, and the velocity structure calculated by *Bower and Hogg* [1996], based on

the same data, closely resembles what we find at 52°W. From the observations just east of our line, *Hendry* [1993] found an average Gulf Stream transport of 100 Sv, though it occasionally reached 160 Sv. He also noted that bottom-intensified bursts of westward flow north of 41°N (his "DWBC") corresponded to seaward movement of the Gulf Stream from its median location (40.2°N for the north edge): this is the situation we observe at 52°W, where the Gulf Stream's north edge is at 38.7°N, and the westward flow north of the warm core ring, excluding the Labrador Current, exceeds that found by Hendry (20.9 Sv at 52°W versus 17 Sv). There is little with which to compare our estimate of the southern recirculation gyre other than *Richardson* [1985], who estimated a southern countercurrent of magnitude 29 Sv between 35°–37°N, of which 12 Sv was believed to be recirculated as eastward flow farther south, leaving 17 Sv to enhance the deep Gulf Stream. Our transports are considerably larger, with a total of 106 Sv of deep water flowing eastward in the Gulf Stream and 76 returning westward between 36° and 37.5°N. However, note that summing the transports of the Labrador Current (−8.6 Sv), DWBC (−12.5 Sv), NRG (−33.4 Sv), deep Gulf Stream (106 Sv), and southern recirculation gyre (−76 Sv) yields a net westward transport north of 36°N of 24 Sv for these waters, compared to 25 Sv found by *Richardson* [1985]. The 55°W array discussed in the work of *Hogg* [1992] and *Bower and Hogg* [1996] extended only to 37°N and as such did not illuminate the nature of the southern recirculation at this longitude.

[32] South of the Gulf Stream system, the velocity and transport fields are more difficult to interpret. The westward flow from 33.5°–36°N is nearly equal in magnitude to the eastward transport directly to the south, from 30°–33.5°N, with top-to-bottom transport of about 80 Sv; the zero velocity line between the two opposing bands also separates the broad CFC maximum in the westward flow, emanating southward from the northern boundary at 1000–2000 m depth, from smaller isolated maxima in the eastward band. The smooth geostrophic field does not capture the same details of the velocity distribution as does the LADCP velocity field. The latter (Figure 2) indicates a narrow band of eastward flow coinciding with the isolated CFC maximum near 31°N, 1500 m, and westward flow directly to the north, coinciding with the relative minimum in CFC-11. Along 66°W, a similar CFC maximum occurs at about 31°N, 1500 m depth, which exceeds the values found at 52°W: 1.2 pmol kg^{-1} at 66W compared to 0.8–1 pmol kg^{-1} at 52°W. As at 52°W, the smooth velocity field resulting from the inverse at 66°W indicates westward flow, while the LADCP velocities are eastward in this middepth range for latitudes of 29–31°N. A rather convoluted circulation pattern would be required to explain the relative distribution of CFC extrema and the velocity fields at 52° and 66°W, if the features were continuous zonally. Such a pattern is difficult to reconcile with the f/H contours for this region. It is likely, however, that the CFC signal at stations 22–26, in an eastward flow of deep water recirculated from the DWBC beneath the Gulf Stream, does not flow around the tail of the Grand Banks into the Newfoundland Basin, but instead turns southward and then back westward, crossing the 52°W section at stations 30–32 (latitude 34°–35.5°N). Such a scheme is consistent with recent work by *Getzlaff et al.* [2004], which suggests that DWBC water should be found at these latitudes along 50°W. Complicating matters somewhat is the fact that LADCP velocities in much of the deep water indicate rather significant departures from strictly zonal flow, at these latitudes as well as farther south. For example, the flow at 2500 m between 30° and 35°N is more southward than eastward.

5.3. Interior Circulation and Southern Boundary Currents

[33] South of 30°N, to about 12°N, the geostrophic velocity field is characterized by broad regions of westward flow punctuated by narrow bands of eastward flow at 23°N and 15°N. The eastward flow at 23°N, which occurs in both inverse solutions (Figure 13), is the location of station pair 48–49, which was noted in section 3 because the velocity added by the inverse was large, 8.6 cm s^{-1} (5.9 cm s^{-1} in the case where only mass was conserved; see Figure 5c). LADCP velocities at 23.5°N have an eastward component between 2000 and 4700 m (Figure 2), but the flow is actually southeastward between 2500 and 3000 m, and northeastward from 3500 to 4000 m (not shown). Indeed, throughout this broad interior region, the LADCP data indicate significant meridional components to the velocity throughout the water column, making it difficult to interpret the two-dimensional velocity field shown in Figure 12. At 15°N, where we find the other band of eastward flow, LADCP data are unfortunately lacking; note, however, that this is the location of a strong property front in the deep water along isopycnals, with characteristics of older, less recently ventilated water occurring on the offshore side of the front. For example, between 3000 and 4500 m, silicate values increase by about 5–6 μmol kg^{-1} along density surfaces at 15°N.

[34] Observing that this pattern exists throughout the tropical western Atlantic, with the characteristics of older water coinciding with the Mid-Atlantic Ridge (MAR), *Mauritzen et al.* [2002] have proposed that it is the result of enhanced mixing of AABW into the overlying waters, due to the rough topography of the ridge. At 52°W, the situation is somewhat different because our section does not approach the MAR perpendicularly, nor even impinge directly on it. However, Researcher Ridge, which protrudes westward from the MAR near 16°N and lies just eastward of our section, may be the location of the enhanced mixing producing the property front on the 52°W section. We hypothesize that the westward flow north of 15°N carries older properties from regions of rougher topography to where they are observed in the section, while the band of eastward flow at 15°N maintains the younger water properties observed directly south of the front. This effect does not seem to be limited to the single front at 15°N: numerous isolated extrema indicate interspersal of older, higher silicate and lower CFC AABW with younger, lower silicate and higher CFC overflow water probably originating in the southern DWBC. For example, the bolus of high silicate water near 13°N at 3300 m appears from Figure 12 to lie in weak eastward flow, but the LADCP data (Figure 2) indicate westward flow for this patch, too, suggesting its origin could lie to the east, near the MAR.

[35] The southern DWBC hugs the continental slope between 8.1° and 9.4°N, with a width of about 165 km

and a total transport in layers 10–17 of 64 Sv (Table 2). All along the western boundary in the tropics, numerous studies have found high DWBC transports (up to 40 Sv), with compensating westward flow offshore, so that the net equatorward transport of these waters more nearly matches the expected magnitude of the meridional overturning cell in the North Atlantic, some 15–20 Sv. Moreover, based on its water properties, the westward flow evidently consists of recirculating water from the boundary current, and it has been hypothesized that one or more recirculating gyres are permanent features of the deep circulation in this area [*McCartney*, 1993; *Friedrichs and Hall*, 1993; *Friedrichs et al.*, 1994]. Our observations do not conform to this pattern. First of all, the boundary current transport itself is much higher than observed elsewhere along the boundary; second, although some weak westward flow occurs between the boundary and 15°N, where properties such as relatively high oxygen and CFCs appear to be fairly uniform and only partially diluted from their values in the DWBC itself, net deep equatorward transport integrated northward from the southern boundary remains high to that point (Figures 13 and 14). The water that returns westward, between 15.5° and 18.5°N, has properties characteristic of much older, less recently ventilated water, as discussed above.

[36] To further investigate this feature, we have used the LADCP observations near the southern boundary, which are continuous for stations 62–91 (7.1°–14.3°N), to estimate a deep stream function analogous to that calculated from the geostrophic velocity field. Integrating all the transport below 1300 m (the approximate depth of the top of layer 10), we find a net DWBC transport of about 51 Sv, still larger than usually observed; but the westward return flow occurs between 11° and 13°N, where properties are more homogenized and less diluted from the boundary current values. The net equatorward transport from the southern boundary to 13°N is 11.8 Sv as calculated in this manner. Similarly, the geostrophic field referenced to the ADCP data, and then corrected with a uniform velocity to balance overall mass, also indicates westward return flow occurring from 9.5° to 14°N. The DWBC transport in this case is 64 Sv, and net equatorward transport between the boundary and 14.2°N is 16 Sv (of course, this solution does not conserve mass and silicate in individual density layers); and the solution conserving mass in individual layers achieves a boundary current transport of 65 Sv, with 33 Sv recirculating westward between 9.5° and 13°N. The differences between these solutions and the final solution shown in Figure 12 can be achieved with rather small differences in absolute velocities. For example, the average velocity difference, weighted by density and area, between the final solution and the solution that achieves overall mass balance with a uniform velocity is 0.02 m s^{-1} over the latitude range 10°–14.3°N, leading to a net transport difference in the deep water of 38 Sv in this range. The difference between the two inverse solutions over the same range is just 0.01 m s^{-1}, corresponding to a cumulative transport offset of 20 Sv. While it might be surmised that the shift of the westward flow from south of 15°N to north of there is somehow associated with the confinement of high silicate AABW to the south of 15°N, we found that relaxing the silicate conservation constraints in layers where the mean silicate values are highest did not materially change the solution.

[37] There are two possible resolutions to this apparent discrepancy. The bulk of the difference in the transport stream functions for the different inverse solutions occurs near 12°N, where the top-to-bottom westward flow is narrower (and weaker) for the silicate-conserving solution than for the others. This could have been an anomalous condition that occurred during the occupation of the section; thus, this circulation pattern could still be consistent with the water property distribution, since the latter results from a long-term average circulation, rather than the instantaneous velocity. Alternatively, it is possible that silicate, and even mass, might not be conserved in the individual layers over the relatively short time frame of the cruise (3 weeks), so that the solution conserving mass only (either in individual layers or simply overall) adequately represents the flow field. In any case, although the cumulative mass transport differs appreciably among the solutions considered here, the basic structure of the velocity field itself looks quite similar for various cases. Hence we are confident that this work gives a faithful rendition of the true velocity field at the time of the cruise; our results for the DWBC at both ends are likely to be particularly robust, inasmuch as the inverse makes only small adjustments to the velocities in these locations, O(1–2 cm s^{-1}).

6. Heat and Freshwater Fluxes

[38] We now consider the implications of the layer mass transport imbalances of Figures 11 and 14 in light of the heat and freshwater fluxes for the ocean volume to the west of 52°W. In section 4, we acknowledged that, though we imposed mass conservation in each of 17 density layers within certain a priori bounds, air-sea buoyancy fluxes over the western North Atlantic may indeed produce conversion of one density class to another, leading to mass transport imbalances in the affected layers. In particular, our final solution (Figure 11) indicates net inflow of warm surface waters into the box (the oceanic volume west of 52°W), with net outflow significantly different from zero in layers 5:7 and 16. *Joyce et al.* [2001] found a similar pattern at 66°W, but with outflow occurring in layers 6 through 8, and none occurring in layer 16. They pointed out that the densest water exposed to wintertime air-sea buoyancy fluxes west of 66°W is a mode water found in the Mid-Atlantic Bight whose water properties correspond to the density of layers 7–8. They concluded that the implied overturning circulation was consistent with the results of the inverse.

[39] Using the results of the inverse, and allowing for errors in the initial reference velocity of up to 0.1 m s^{-1}, we estimate a net heat exchange across our section of −0.66 to −0.87 PW (1 PW = 10^{15} W) (about −43.4 W m^{-2} for the velocity field in Figure 12). The negative sign indicates that heat is imported into the oceanic volume west of 52°W, where it is subsequently lost to the atmosphere. Most of this heat flux is the result of the mass imbalance in layer 1: i.e., warm waters flow in through the south, but are largely converted to colder density classes before flowing back eastward in the northern half of the section. Additionally, the layer 1 water that flows eastward in the Gulf Stream, for example, is slightly cooler than the surface waters flowing westward at the southern end of the section; this difference

would be exaggerated in winter, increasing the heat exchange, because Gulf Stream waters are much cooler in winter, while the southern inflow remains warm. Hence we probably underestimate the annual heat exchange. Still, it is useful to compare our result with an estimate derived from the mean annual air-sea heat exchange integrated over the ocean surface west of 52°W. Using the *da Silva and Levitus* [1994] values from Comprehensive Ocean-Atmosphere Data Set (COADS), we obtain a total heat loss from ocean to atmosphere over this region of −0.45 PW, or about -25.6 W m^{-2}. The differences in the two estimates amount to about 18 W m^{-2}. This is similar to the difference noted by *Joyce et al.* [2001] for the same comparison at 66°W, and they argue that it is within the uncertainty estimates of the COADS heat flux product.

[40] Freshwater flux crossing the section into the closed volume to the west should, in the mean, be equal in magnitude to the excess of evaporation over precipitation plus runoff over that volume. Knowledge of these fluxes and their divergences is critical to understanding the global hydrologic cycle, and estimates based on direct oceanic measurements provide an independent assessment for comparison with meteorologically based estimates. Following *Joyce et al.*'s [2001] formulation, we find a westward flux of freshwater across 52°W of 0.45–0.65 Sv, indicating that evaporation dominates over precipitation plus runoff for the enclosed volume west of 52°W. The annual mean for the same quantity, calculated again from *da Silva and Levitus* [1994], is 0.33 Sv, which like the heat flux is about 40% less than our estimate. Of course, this quantity is subject to seasonality as is the heat flux, both in the precipitation/evaporation balances and in the river runoff. The latter includes the Amazon, which empties into the Atlantic just east of our section at the southern end, and which almost certainly has an influence on the freshwater flux calculation. A complete understanding of the various seasonal influences is beyond the scope of this paper, however, and here we simply note that the magnitudes of both the heat and freshwater fluxes calculated for the 52°W section are larger than the fluxes calculated by Joyce et al. for 66°W by an amount roughly proportional to the surface area of the ocean west of the respective lines.

[41] **Acknowledgments.** This work was supported by NSF grants OCE95-29607, OCE 95-31864, OCE98-18266, and OCE-0219644. We also wish to thank Alonso Hernandez-Guerra for his assistance in creating and implementing the inverse model, and Elizabeth Stokes for preparing the manuscript. This is contribution 11055 of the Woods Hole Oceanographic Institution and number 6662 from Lamont-Doherty Earth Observatory.

References

Bower, A. S., and N. G. Hogg (1996), Structure of the Gulf Stream and its recirculations at 55°W, *J. Phys. Oceanogr.*, *26*, 1002–1022.

Csanady, G. T., and P. Hamilton (1988), Circulation of slopewater, *Cont. Shelf Res.*, *8*, 565–624.

da Silva, A. M., and S. Levitus (Eds.) (1994), *Atlas of Marine Data 1994*, vol. 1, *Algorithms and Procedures*, 83 pp., U.S. Dept. of Comm., Washington, D. C.

Donohue, K. A., and J. M. Toole (2003), A near-synoptic survey of the Southwest Indian Ocean, *Deep Sea Res. Part II*, *50*(12–13), 1893–1931.

Fischer, J., and M. Visbeck (1993), Deep profiling with self-contained ADCPs, *J. Atmos. Oceanic Technol.*, *10*, 764–773.

Fofonoff, N. P., and M. M. Hall (1983), Estimates of mass, momentum, and kinetic energy fluxes of the Gulf Stream, *J. Phys. Oceanogr.*, *13*, 1868–1877.

Friedrichs, M. A. M., and M. M. Hall (1993), Deep circulation in the tropical North Atlantic, *J. Mar. Res.*, *51*, 697–736.

Friedrichs, M. A. M., M. S. McCartney, and M. M. Hall (1994), Hemispheric asymmetry of deep water transport modes in the western Atlantic, *J. Geophys. Res.*, *99*(C12), 25,165.

Getzlaff, K., J. H. Dengg, and C. W. Boning (2004), Pathways of deep water export from the subpolar to the subtropical gyre in the North Atlantic: Eulerian and Lagrangian views, *Eos Trans. AGU*, *84*(52), Ocean Sci. Meet. Suppl., Abstract OS31E-03.

Hall, M. M., and R. S. Pickart (2003), Boundary current system at 52°W in the North Atlantic, *Eos Trans. AGU*, *84*(52), Ocean Sci. Meet. Suppl., Abstract OS21F-08.

Hendry, R. (1993), Currents south of the Grand Banks at 50°W: Estimates of mass transport, in *The North Atlantic Current System: A Scientific Report*, pp. 111–112, Woods Hole Oceanogr. Inst., Woods Hole, Mass.

Hogg, N. G. (1992), On the transport of the Gulf Stream between Cape Hatteras and the Grand Banks, *Deep Sea Res.*, *39*, 1231–1246.

Hogg, N. G. (2000), Low-frequency variability on the western flanks of the Grand Banks, *J. Mar. Res.*, *58*, 523–545.

Hogg, N. G., R. S. Pickart, R. M. Hendry, and W. M. Smethie (1986), The northern recirculation gyre of the Gulf Stream, *Deep Sea Res. Part I*, *33*, 1139–1165.

Joyce, T. M. (1994), WOCE operations manual, Rev. 1, *WHP OFF. Rep. WHPO-91-1, WOCE Rep. 68/91*, Woods Hole Oceanogr. Inst., Woods Hole, Mass.

Joyce, T. M., and P. Robbins (1996), The long-term hydrographic record at Bermuda, *J. Clim.*, *9*, 3121–3131.

Joyce, T. M., R. S. Pickart, and R. C. Millard (1999), Long-term hydrographic changes at 52° and 66°W in the North Atlantic subtropical gyre and Caribbean, *Deep Sea Res. Part II*, *46*, 245–278.

Joyce, T. M., A. Hernandez-Guerra, and W. M. Smethie (2001), Zonal circulation in the NW Atlantic and Caribbean from a meridional World Ocean Circulation Experiment hydrographic section at 66°W, *J. Geophys. Res.*, *106*(C10), 22,095–22,113.

Lazier, J., R. Hendry, A. Clarke, I. Yashayaev, and P. Rhines (2002), Convection and restratification in the Labrador sea, 1990–2000, *Deep Sea Res., Part I*, *49*, 1819–1835.

Mauritzen, C., K. L. Polzin, M. S. McCartney, R. C. Millard, and D. E. West-Mack (2002), Evidence in hydrography and density fine structure for enhanced vertical mixing over the Mid-Atlantic Ridge in the western Atlantic, *J. Geophys. Res.*, *107*(C10), 3147, doi:10.1029/2001JC001114.

McCartney, M. S. (1993), Crossing of the equator by the deep western boundary current in the western Atlantic Ocean, *J. Phys. Oceanogr.*, *23*, 1953–1974.

McLellan, H. J. (1957), On the distinctness and origin of the slope water off the Scotian shelf and its easterly flow south of the Grand Banks, *Fish. Res. Board Can.*, *14*, 213–239.

Pickart, R. S., and W. M. Smethie Jr. (1998), Temporal evolution of the Deep Western Boundary Current where it enters the sub-tropical domain, *Deep Sea Res. Part I*, *45*, 1053–1083.

Pickart, R. S., T. K. McKee, D. J. Torres, and S. A. Harrington (1999), On the mean structure and interannual variability of the slopewater system south of Newfoundland, *J. Phys. Oceanogr.*, *29*, 2541–2558.

Richardson, P. L. (1985), Average velocity and transport of the Gulf Stream near 55°W, *J. Mar. Res.*, *43*, 83–111.

World Ocean Circulation Experiment (WOCE) (1998), Mean surface wind fields from ERS-AMI and ADEOS-NSCAT microwave scatterometers, Paper presented at WOCE Conference, World Ocean Circ. Exp., Halifax, Canada, May.

Wunsch, C. (1996), *The Ocean Circulation Inverse Problem*, 442 pp., Cambridge Univ. Press, New York.

M. M. Hall, T. M. Joyce, R. S. Pickart, and D. J. Torres, Physical Oceanography Department, Woods Hole Oceanographic Institution, Woods Hole, MA 02543, USA. (mhall@whoi.edu)

W. M. Smethie Jr., Lamont-Doherty Earth Observatory, Columbia University, Palisades, NY 10964, USA.